# The contribution of an urban gravity survey to the determinable perspective of Athens city (Greece) underground structure

**Spyridon Dilalos, John D. Alexopoulos**

National and Kapodistrian University of Athens, Department of Geology and Geoenvironment, Division of Geophysics-Geothermic, Panepistiomioupoli Zografou, Greece

sdilalos@geol.uoa.gr, jalexopoulos@geol.uoa.gr

## Abstract

An urban gravity survey with more than 1,120 measurements was carried out in order to adumbrate the deeper subsurface of Athens city basin. The aim was to gather quantitative information of the subsurface structure derived from the acquisition of gravity measurements. At first, a gravity base network has been established for the data collection. The standard data reduction has been carried out along with an additional Building Correction that has been calculated due to the urban characteristics. Subsequently, the residual anomaly was isolated with the contribution of the Fourier filters. The Euler deconvolution has been applied, with two different techniques, providing depth solutions for the residual maps. Based on these maps, we managed to retrieve quantitative information for the depths of anomalous sources, ranging between 500 and 3,760 meters. Moreover, unconstrained 3D density models of the area have been constructed in order to obtain a good image of the subsurface, up to depths of 4,500 meters. For each 3D density model, we provide a couple of images; one illustrating only the structures of lower densities and one other only with the structures of higher densities, in an effort to delineate better the tectonic structures. Finally, two geophysical-geological profiles (2.75D) have been constructed, along which the geotectonic regime of the subsurface seems to be adumbrated in a better way. Major known tectonic structures of Athens basin have been identified beneath the surface.

**Keywords**: 2.75D Interpretative sections, 3D density models, Euler deconvolution depths, Gravity bases, Urban gravity measurements

## 1. Introduction

The metropolis city of Greece is located in Athens basin, where 4 million people live and work. Taking into consideration the major damage caused by the devastating earthquake of 7$^{th}$ September 1999 ($M_w$=5.9R), the need for further and deeper investigation of the geological structure of the subsurface came up. Especially in such urban and fully residentially developed areas, the knowledge on the existence of concealed active faults is absolutely valuable. The

damage distribution of an earthquake is known to depend on the tectonic pattern of the area. A small problem arises due to the fact that the artificial surfaces (buildings, roads, bridges etc) dominate along Athens, making the geological research more difficult.

The geophysical methods can overcome this difficult situation by retrieving information for the deep subsurface. Taking into account the land cover data presented in Figure 1, provided by CORINE 2012 project (European Environment Agency, 2012), the areas of artificial surfaces cover a 54.5% of our study area (Dilalos, 2018). The land gravity survey seems the most suitable method for the deep geotectonic investigation. Gravity measurements have been applied widely the last few years contributing to the investigation of basin structure (Khamies and El-Tarras, 2010; Nasr *et al.,* 2011; Koumetio *et al.,* 2012; Hosseini *et al.,* 2013; de Castro *et al.*, 2014; Dilalos *et al*., 2019a; 2019b).

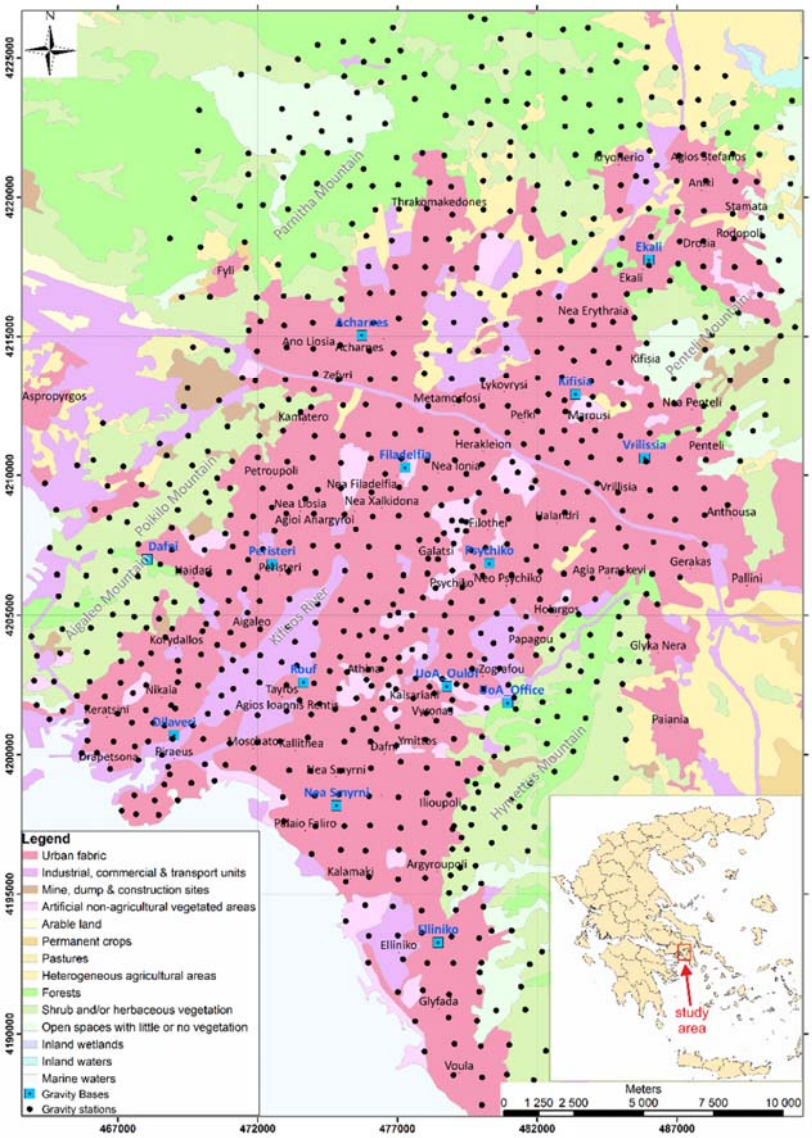


**Figure 1.** Simplified land cover map of the study area, based on CORINE 2012 data. An index map is also provided.

One of the methods used in this paper is the Euler deconvolution, successfully applied in the past by other authors (FitzGerald *et al.,* 2004*;* Naouali *et al.,* 2011; Nasr *et al.,* 2011; Khalil *et al.,* 2014; Curto *et al.,* 2015; Martins-Ferreira *et al*., 2018; Dilalos and Alexopoulos, 2019b). Practically, Euler methods are considered as derivatives method of first, second or even third order. The method uses three orthogonal gradients of the gravity field along with the field itself, in order to determine the location and the depth of the target. The obtained results provide us with the necessary information which will lead to the production of a set of maps, illustrating the locations and depths of the geologic sources of gravity anomalies that have been identified in grid-based gravity data. This information can help us understand better the seismotectonic structure of Athens basin.

In the context of outlining the basin subsurface structure, we will take advantage of the quantitative gravity interpretation and its 3D density models that will be produced. Through their analysis, we can try to define some specific parameters, such as the location, depth, shape and density contrast of the geological bodies. Thus, gravity interpretation cannot be characterized by its uniqueness and absolute solution, due to its ambiguity problem, but any additional, data can constrain the quantification errors and limits. The real aim of the gravity inversion is to define model bodies that could realistically correspond to geological and tectonic structures.

This paper is structured in the following 4 sections. In Section 2 we provide detailed geological and tectonic information of the study area, which is essential for the final interpretation of the gravity results. In Section 3 all the steps of the gravity method are presented, beginning from the establishment of the gravity base network and the acquisition of the gravity data, then the data reduction procedures and finally the application of the Euler method, the production of the 3D density models along with the 2.75D geological-gravity sections. In Section 4, a detailed presentation and discussion of the 2.75D geological-gravity sections is provided, in order to fully understand them. Finally, in Section 5 the results of the gravity survey and the geological interpretation are presented, along with the new insights for the area.

## 2. Geological and tectonic setting

The Athens basin covers an area of almost 360 km$^2$, bounded by the mountains *Hymettus* (East), *Parnitha* (North), *Penteli* (Northeastern) and *Aigaleo-Poikilo* (West). Its geology has been studied by many authors due to its complication (Lepsius, 1893; Freyberg, 1951; Marinos *et al*. 1971; 1974; Niedermayer, 1971; Sabatakakis, 1991; Lozios, 1993; Lekkas and Lozios, 2000; Mariolakos *et al.*, 2000; Papanikolaou et al., 2002; 2004; Krohe *et al*., 2010). `

In Figure 2, we provide a simplified geology regime of the area (Dilalos, 2018; Dilalos *et al*., 2019a) mostly based on this up-to-date geotectonic study by Papanikolaou *et al.,* (2002) but completed and combined with some of the existent studies where there was no coverage. The geological regime is quite complicated. An autochthonous metamorphic geotectonic unit covers the eastern margin (*Penteli* and *Hymettus* Mountains), while an allochthonous unit

(“*Ypopelagoniki*”) structures the western margin (Aigaleo and Poikilo mountains). Finally, there are two more local allochthonous units, “*Alepovouni Unit*” and “*Athens Unit*”.

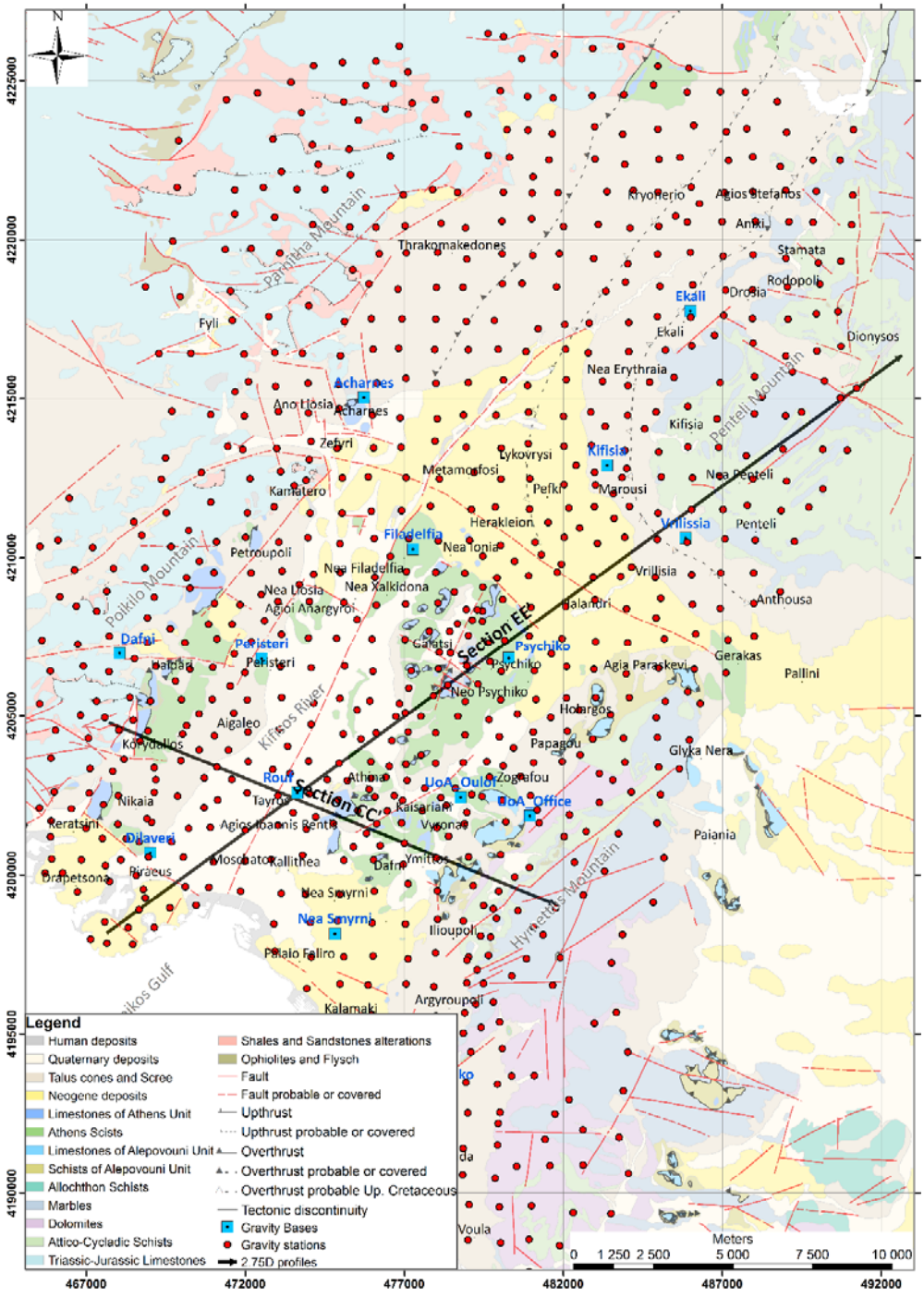


**Figure 2.** Geological and tectonic map along with the locations of the gravity stations and gravity bases. The locations of the two interpretative geological-gravity profiles (§3.5) are also illustrated.

The autochthonous metamorphic unit includes dolomites but also marbles and shales, as continuous overlaying layers. The “*Ypopelagoniki*” unit is comprised of the Triassic-Jurassic limestones and clastic formations from Paleozoic at its base. The “*Athens Unit*” has practically

two main parts, the upper one with limestones and the lower one (known as "*Athens Schists*"), which is a geological mélange including shales, sandstones, phyllites, limestones and marls. The "*Alepovouni" Unit* consists of limestones in its upper part, while schists and phyllites appear in the base, because of its low metamorphism. It is located tectonically between the autochthonous metamorphic unit and the "*Athens"* one.

The biggest part of the basin is covered by the post-alpine geological formations, apart from the remaining hills in the center (*Tourkovounia, Filopappou, Lycabettus, Ardittou, Acropolis, Kokkou*), where the "*Athens Unit"* dominates. The research of Papanikolaou *et al.,* (2002) mentions more than ten different Quaternary and Neogene geological formations, which were unified in groups (Dilalos, 2018; Dilalos *et al*., 2019a) for a better handling. Because of their existence, it is difficult to understand with no doubt the geotectonic regime of the basin.

The alpine tectonic regime is controlled mainly by low-angle fault zones, known as part of the **West Cycladic Detachment System** (Iglseder *et al*., 2011; Lekkas *et al*., 2011; Grasemann *et al*., 2012; Seman *et al*., 2012; 2013; Coleman *et al*., 2018). The *Alepovouni Unit* is delimited by two low-angle fault zones, one with the relative autochthonous underlying Metamorphic Unit dipping to Northwest. The tectonic contact between the *Alepovouni and Athens* Units is considered to be a major tensile detachment zone, where metamorphic formations adjust to unmetamorphic ones, leading to the rise of the metamorphic up to the surface (Katsikatsos, 1977; Katsikatsos *et al.*, 1986; Papanikolaou, 1986; Xypolias *et al.,* 2003).

## 3. Gravity survey

### *3.1 Establishment of gravity bases and data acquisition*

In the past, several authors (e.g. Berg and Thiruvathukal, 1965; Robertson, 1965; Warsi, 1989; Lagios, 1985; Csapó and Völgyesi, 2002; Krynski *et al.*, 2013; Srivastava *et al*., 2015; Dilalos and Alexopoulos, 2019a) have discussed the establishment of absolute gravity bases networks, in several areas of the world, mostly for quite larger areas.

Taking into account the traffic jam of this over-populated metropolis and the increased time that we would spend moving among the stations and the base re-measurements, we planned and established very cautiously a gravity base network (Dilalos and Alexopoulos, 2019a), distributing spatially **fourteen (14) gravity bases** (Fig. 2-blue squares) in a way that would be less time-consuming for the base loops. Each established base (Table 1) was characterized by 3 engraved permanent marks on the ground for more enduring results. In that way, the re-measurements would always be at the exact same point. Detailed sketches and photographs of each gravity base and its surrounding stable structural characteristics (columns, balusters, stairs, walls, yards etc.) were kept. The established gravity base network is referred to the IGSN'71 datum (Morelli *et al*., 1974) as it was tied to an existing base in the University of Athens (Hipkin *et al*., 1988).

Taking into consideration the complex geology of the area and the urban characteristics, we planned the gravity survey on a grid. Because of the urban character of the study area, the gravity grid had to be organized very carefully, taking advantage of high-accuracy space images. The station grid spacing had been set primarily to 1 km and then some stations had been added in between the first ones, in order to clarify the status of some ambiguous areas. All the campaigns were carried out during summer (2013-2015) in order to minimize the time consumed between the stations and the bases (reduced traffic jam). The gravity meter LaCoste & Romberg G-496 was used for the data acquisition, with an accuracy of ±0.01 mGal. The gravity database is comprised of 1.122 gravity stations (Fig. 2).

In order to calculate the necessary coordinates of each gravity station and base with high precision, we used Differential Global Positioning System (dGPS), compiled by two different, dual-frequency *TopCon HiperPro* GPS antennas. The *static* technique had been chosen, because of the long distances and the blear of the buildings. In this way, the achieved accuracy of the calculated coordinates was of the centimeter scale. The coordinates were calculated in the Hellenic Geodetic Reference System (EGSA'87).

| **Gravity base name** | **Absolute gravity (mGal)** | **Maximum Deviation (mGal)** | **Easting (Egsa '87,m)** | **Northing (Egsa '87, m)** | **Elevation (m)** |
|---|---|---|---|---|---|
| UoA_Office | 980,010.75 | ±0.00 | 480,948.310 | 4,201,848.100 | 252.000 |
| UoA_Oulof | 980,029.86 | ±0.03 | 478,772.001 | 4,202,445.816 | 134.792 |
| Rouf | 980,049.35 | ±0.04 | 473,639.680 | 4,202,590.600 | 20.239 |
| Psychiko | 980,017.27 | ±0.03 | 480,288.710 | 4,206,831.900 | 179.091 |
| Nea Smyrni | 980,043.88 | ±0.04 | 474,819.600 | 4,198,156.400 | 42.662 |
| Peristeri | 980,044.15 | ±0.07 | 472,514.450 | 4,206,815.757 | 51.888 |
| Dilaveri | 980,052.98 | ±0.08 | 469,013.766 | 4,200,694.898 | 7.536 |
| Kifisia | 979,991.51 | ±0.04 | 483,373.599 | 4,212,901.998 | 287.379 |
| Filadelfia | 980,029.07 | ±0.04 | 477,276.990 | 4,210,270.695 | 116.118 |
| Elliniko | 980,039.12 | ±0.07 | 478,453.689 | 4,193,259.660 | 80.884 |
| Acharnes | 980,017.08 | ±0.07 | 475,726.609 | 4,215,036.626 | 168.425 |
| Ekali | 979,981.33 | ±0.07 | 485,997.896 | 4,217,756.564 | 344.891 |
| Vrilissia | 979,997.11 | ±0.07 | 485,846.098 | 4,210,619.196 | 269.935 |
| Dafni | 980,031.44 | ±0.05 | 468,050.208 | 4,206,980.671 | 109.281 |

**Table 1**: Established gravity bases in Athens (Fig. 2) along with their determined absolute values

### *3.2 Data processing and reduction*

The data processing and reduction of the gravity measurements have already been presented and analyzed by the authors in the past (Dilalos, 2018; Dilalos *et al.,* 2018; Dilalos *et al.,* 2019a) and for that reason we will present them briefly. The assumed constant density for the Bouguer correction was set up to 2.67 gr/cm$^3$, generally used by several other researchers in the broader area (Casten and Snopek, 2006; Papadopoulos *et al.,* 2007; Makris *et al.*, 2013). Therefore, the Simple Bouguer Anomaly has been calculated and has been presented by Dilalos *et al.,* 2019a. In order to calculate the necessary terrain correction up to a radius distance of 21 kilometers, we

took advantage of the *Gravity and Terrain Correction* extension of *Oasis Montaj* software. Due to the urban characteristics of the survey, we have calculated and added the Building Corrections (Dilalos, 2018; Dilalos *et al.,* 2018) caused by the gravitational attraction of the buildings and infrastructures of the city. The final construction of the Complete Bouguer Anomaly map has been presented and discussed thoroughly by Dilalos *et al.,* 2019a.

Among the existing filtering processes, we chose to proceed to the regional-residual separation with the application of the Gaussian filter with a cutoff wavelength of 500m, that has been applied successfully in several other cases (de Castro *et al.,* 2014; Anudu *et al.,* 2016; Dilalos and Alexopoulos, 2017; Fernandez-Cordoba *et al*., 2017; Dilalos *et al.,* 2019a;). The separation of the regional and residual gravity fields was based on the information provided by the corresponding Power Spectrum Analysis (Dilalos *et al.,* 2019a). Based on its results, two different depths of the anomaly sources seem to have been identified, at 2.06 km and 0.48 km depth. Subsequently, a residual map has been produced (cutoff wavelength 500m) with standard deviation of 0.25 cycles/km (Figs. 4 & 6) and a second residual map of the basement, with standard deviation of 0.02 cycles/km. The first one is mainly for the shallow structures, (Figs. 3 & 5) while the second one ("basement residual") includes the anomaly sources and information from deeper structures of the bedrock.

### *3.3. Euler Deconvolution*

Although Euler deconvolution is mostly applied for the magnetics, it can sometimes be applied successfully for gravity data (Keating, 1998) as an approximation. The only difference is that the calculated depth solutions for the gravity method are located at a deeper level, closer to the center of the mass, in regard with the ones of magnetics.

The outcome of the Euler deconvolution here is a map, illustrating the locations and depths of the geologic sources of gravity anomalies that have been identified in grid-based gravity data, like in several other cases (FitzGerald *et al.,* 2004*;* Naouali *et al.,* 2011; Nasr *et al.,* 2011; Khalil *et al.,* 2014; Curto *et al.,* 2015; Martins-Ferreira *et al*., 2018; Dilalos and Alexopoulos, 2019b). For the best results from Euler deconvolution, Reid *et al.* (2014a; 2014b) discuss the avoidable errors during its application to gravity data and how to determine suitably the required parameters (SI, window size, grid interval etc.). The grid cell of the processed data is important, since the minimum depths defined are about the same as the cell size.

One fundamental parameter for Euler deconvolution is the **Structural Index (SI)** value, which depends on the type of the source body, causing the gravity anomaly. In the context of this paper, we have calculated Euler depth solutions by using values equal to 0 (Figs. 3 & 5) and 1 (Figs. 4 & 6), since both are considered to be close to the fault/contact type that we want to delineate. Of course, the SI=0 is estimated to appear almost the twice the uncertainty of the one for SI=1, which appears depth uncertainty equal to 10% and horizontal one equal to 20%. Although several researchers have used non-integer values such as 0.5 for Structural Index (Slack *et al.,* 1967; Tedla *et al.,* 2011), we decided not to, based on the comments of Reid *et al.* (2012; 2014b).

Additionally, Reid *et al.,* (2014a; 2014b) propose that the SI equal to -1 is the appropriate value for finite contacts and faults in gravity surveys, but it has not been embedded as a possible value in most software and therefore we cannot test its results. The **window size** was set to 15x15 grid points, trying to compromise with all the conflicting requirements (Reid *et al.,* 2014a). This means that it should be as small as possible but also greater than twice the acquired data grid spacing. Simultaneously, it should be greater than half the desired depth of investigation, which here is at least 2-3 kilometers. Moreover, some eliminations of spurious solutions were executed, by setting some acceptable parameters, such as the maximum acceptable distance (7500 m), the maximum depth tolerance (14%) and the maximum horizontal tolerance (35%).

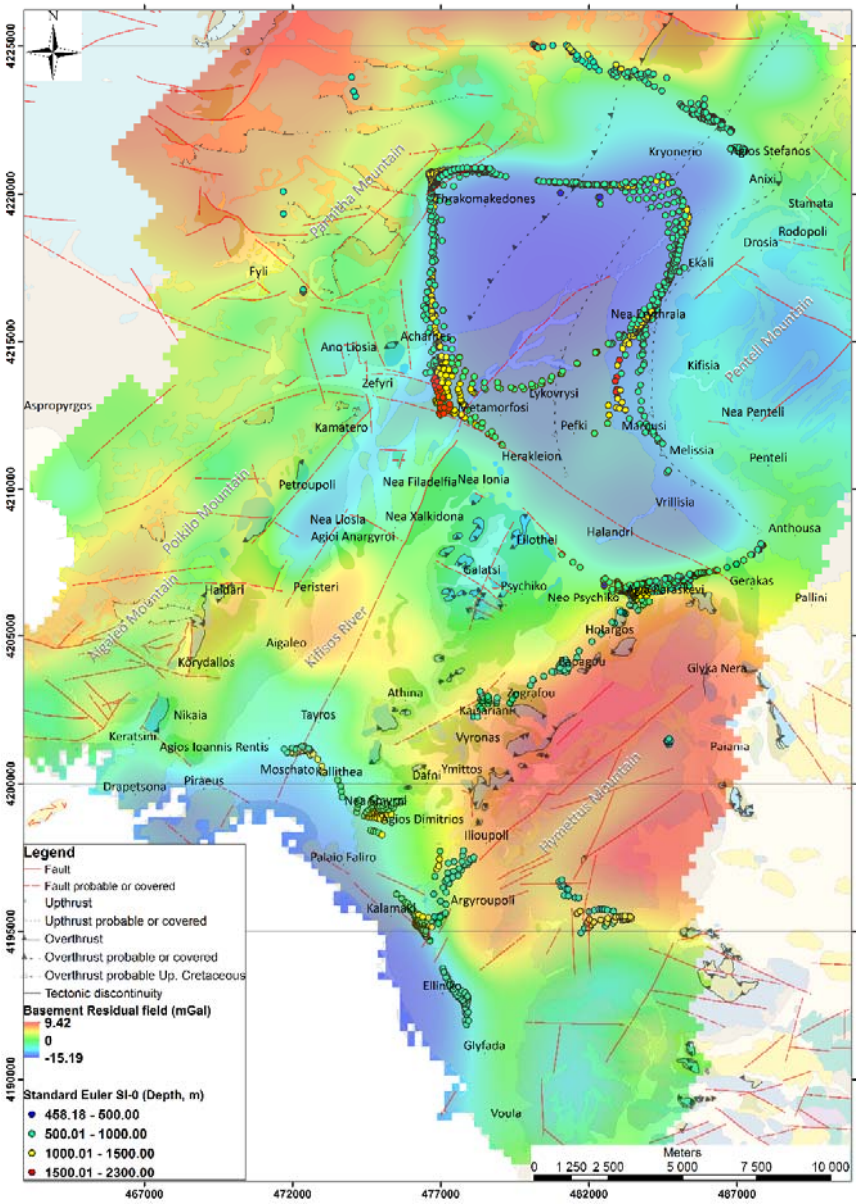


**Figure 3.** Standard Euler solutions (graduated symbols with depth) for SI=0 along with the Residual Map of Athens basin, illustrating the deeper bedrock anomaly sources

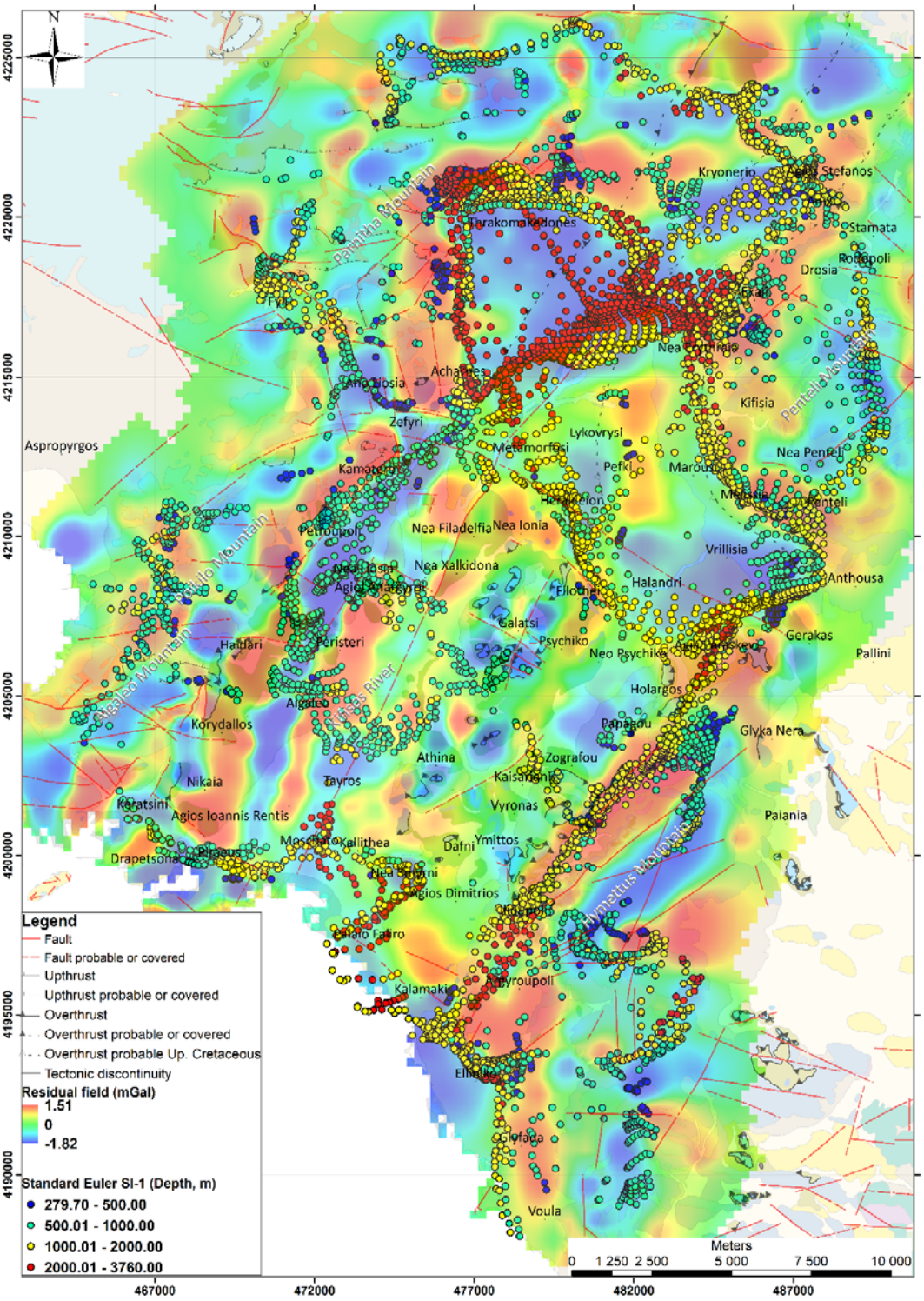


**Figure 4**. Standard Euler solutions (graduated symbols with depth) for SI=1 along with the Residual Map of basement, illustrating the shallow anomaly sources

The Euler deconvolution has been carried out with the *Euler3D* extension of *Oasis Montaj* software and more specifically with two different methods, the *Standard Euler* (Figs. 3-4) and the *Located* one (Figs. 5-6). The second one produces far fewer spurious solutions (Figs. 5-6)

since it is based only at the areas with existing anomalies (picks) in the analytic signal. The input grid data were the residual and the basement residual ones. The generated Euler depth solutions from both input data were merged and presented together in order to have a common image that would lead to an easier evaluation.

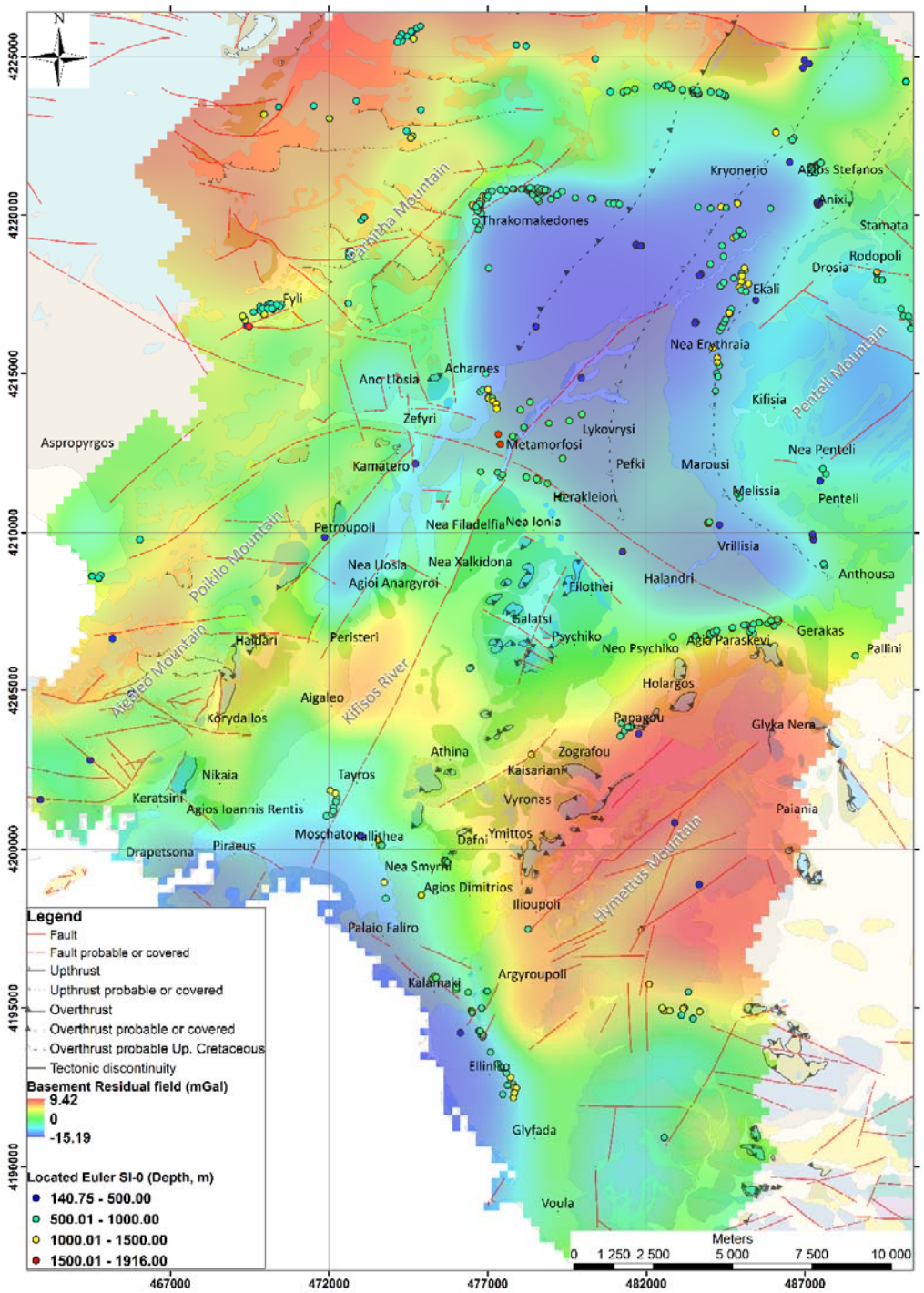


**Figure 5.** Located Euler solutions (graduated symbols with depth) for SI=0 along with the Residual Map of Athens basin, illustrating the deeper bedrock anomaly sources

The produced solutions for the Structural Index zero (0) are located mainly around the main low-gravity spherical area (*Thrakomakedones, Kryoneri, Ekali, Nea Erythraia, Lykovrysi, Acharnes*) observed in the basement residual map, with depths mostly between 500 and 1,500 meters and some deeper (1,500-2,300 m) at the southwest corner. Moreover, we observe solutions of depths ranging from 500 to 1,000 meters along two linear areas. The first area is located at the western foothills of *Hymettus* Mountain, from *Anthousa* to *Kaisariani* and the second one is at the southern foothills of *Parnitha* Mountain, along *Agios Stefanos* and *Drosopigi*. Additionally, solutions for depths from 500 up to 1,500 meters are observed at the southern suburbs of Athens basin, along smaller areas, such as *Agios Ioannis Rentis-Moschato-Kallithea, Nea Smyrni-Agios Dimitrios, Kalamaki-Elliniko* and *Elliniko-Glyfada.* The solutions clusters are more extended and systematic in the Standard Euler technique, while the solutions in the Located Euler are constrained a lot. On the other hand, there are not large differentiates of depths and locations between the two methods.

For Structural Index equal to one (1), the number of the produced Euler solutions is quite higher (Figs. 4 & 6), especially for the ones produced through the Standard Euler procedure. It seems that we have enough correlations between the locations of the solutions and possible or existing fault zones. For SI=1, we can also observe great clusters of solutions around the margins of the main low-gravity area, similar to the SI=0 ones. The calculated depths are bigger, reaching up the 3,760 meters, when the SI=0 gave maximum depths up to 2,300 meters and quite restricted in swarm. Furthermore, the two linear areas of solutions, presented for SI=0 (Figs. 3 & 5), along the foothills of *Parnitha* and *Hymettus* Mountains, also appear with greater calculated depths (up to 3,760 m for *Parnitha Mt* and up to 2,000 m at *Hymettus Mt*.) and expanded in length. This means that the one is running along *Anthousa-Agia Paraskevi-Holargos-Kaisariani-Argyroupoli-Kalamaki* and the other along *Agios Stefanos-Drosopigi*. For the linear areas located in the southern suburbs, we can also observe larger depths.

Beyond the clusters of solutions detected for both Structural Indexes 0 and 1, by setting SI=1 we observe new clusters of solutions, in other areas, located in the central and western part of the basin. More specifically, clusters of solutions for depths 500-1,000 meters are spotted along the zone *Zefyri-Kamatero-Petroupoli-Haidari, Keratsini-Drapetsona-Piraeus, Agioi Anargyroi-Peristeri, Aigaleo-Votanikos-Downtown-Psychiko*, *Penteli* and *Hymettus Mt.* For bigger depths (1,000-2,000 m) along *Nea Penteli-Melissia-Marousi-Nea Erythraia, Agia Paraskevi-Halandri-Herakleion-Metamorfosi-Acharnes*, *Kryoneri-Agios Stefanos* and *Piraeus-Faliro-Moschato*. At the areas of *Fyli* and *Poikilo-Aigaleo* mountains, the depths of solutions range from 500 to 2,000 meters.

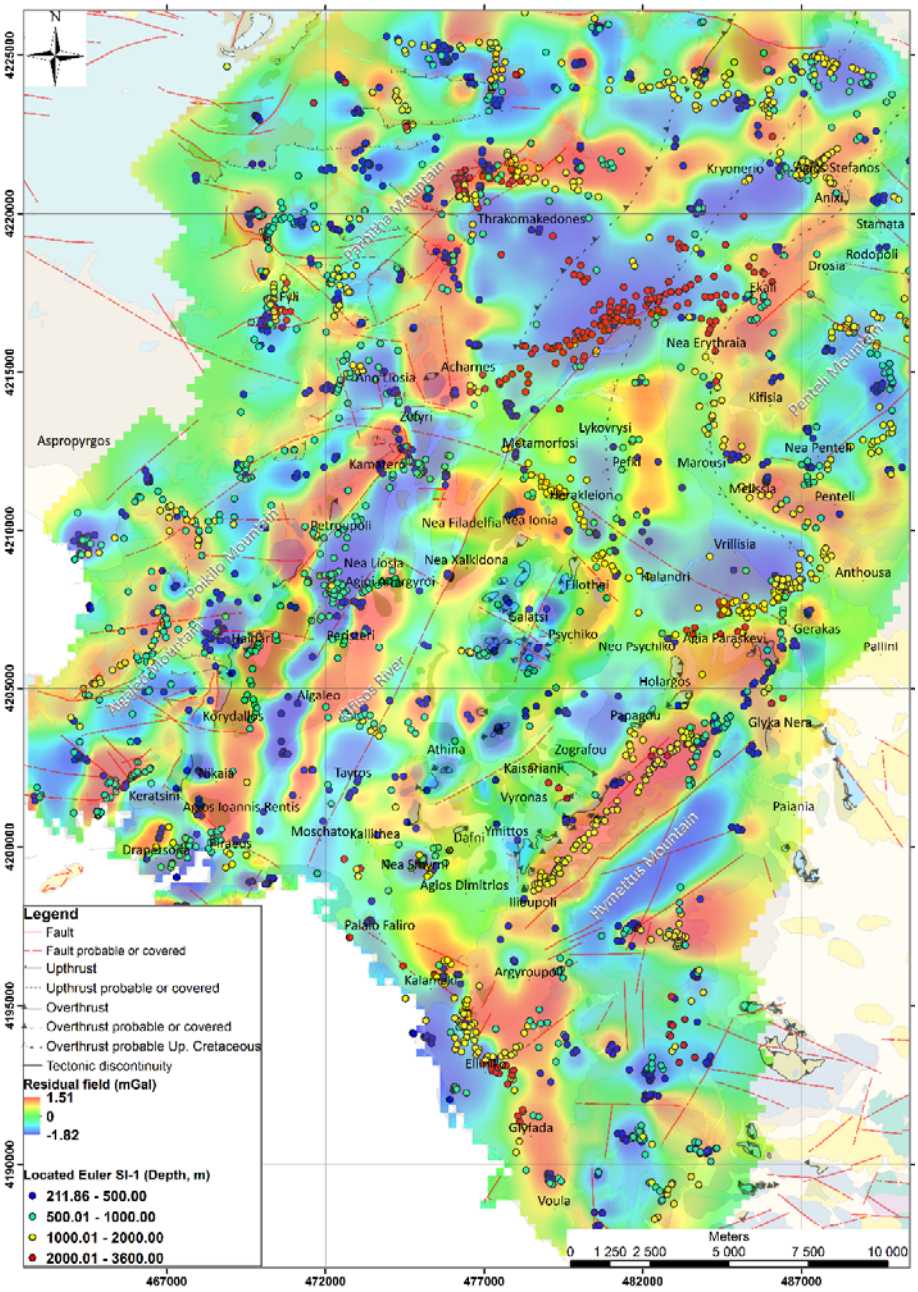


**Figure 6**. Located Euler solutions (graduated symbols with depth) for SI=1 along with the Residual Map of basement, illustrating the shallow anomaly sources

## *3.4 3D density models*

The 3D gravity modelling has been evolved rapidly during the last years (Boszczuk *et al.*, 2011; Choi *et al.*, 2011; Commer, 2011; Prutkin *et al.*, 2011; Wang *et al.*, 2011; Martinez *et al.*, 2013; Azizi and Saibi, 2015; Bersi *et al.*, 2016; Farhi *et al.*, 2016; Damaceno *et al.*, 2017; Wehr *et al.*, 2018). 3D modelling of the gravity data provides us with information concerning the volume and geometry of the anomalous sources that cause gravity anomalies and can be a powerful tool for geological interpretation. The density model is constructed based on a mesh of blocks/cells of

equal dimensions, specified from the beginning, each one characterized by a certain value of density or density contrast.

All the density inversions within the context of this paper have been carried out using the "*VOXI*" Earth modelling module (Azizi and Saibi, 2015; Farhi *et al.*, 2016; Weidmann *et al.,* 2016; Martins-Ferreira *et al*., 2018) of Oasis Montaj by Geosoft. They have been integrated with the defined densities of the geological formations, derived from the application of three different methods (Dilalos, 2018; Dilalos *et al.,* 2019a). Therefore, we managed to determine the density of all the formations, even of the ones compiled of different lithologies, such as the Neogene formations and the Athens Schists.

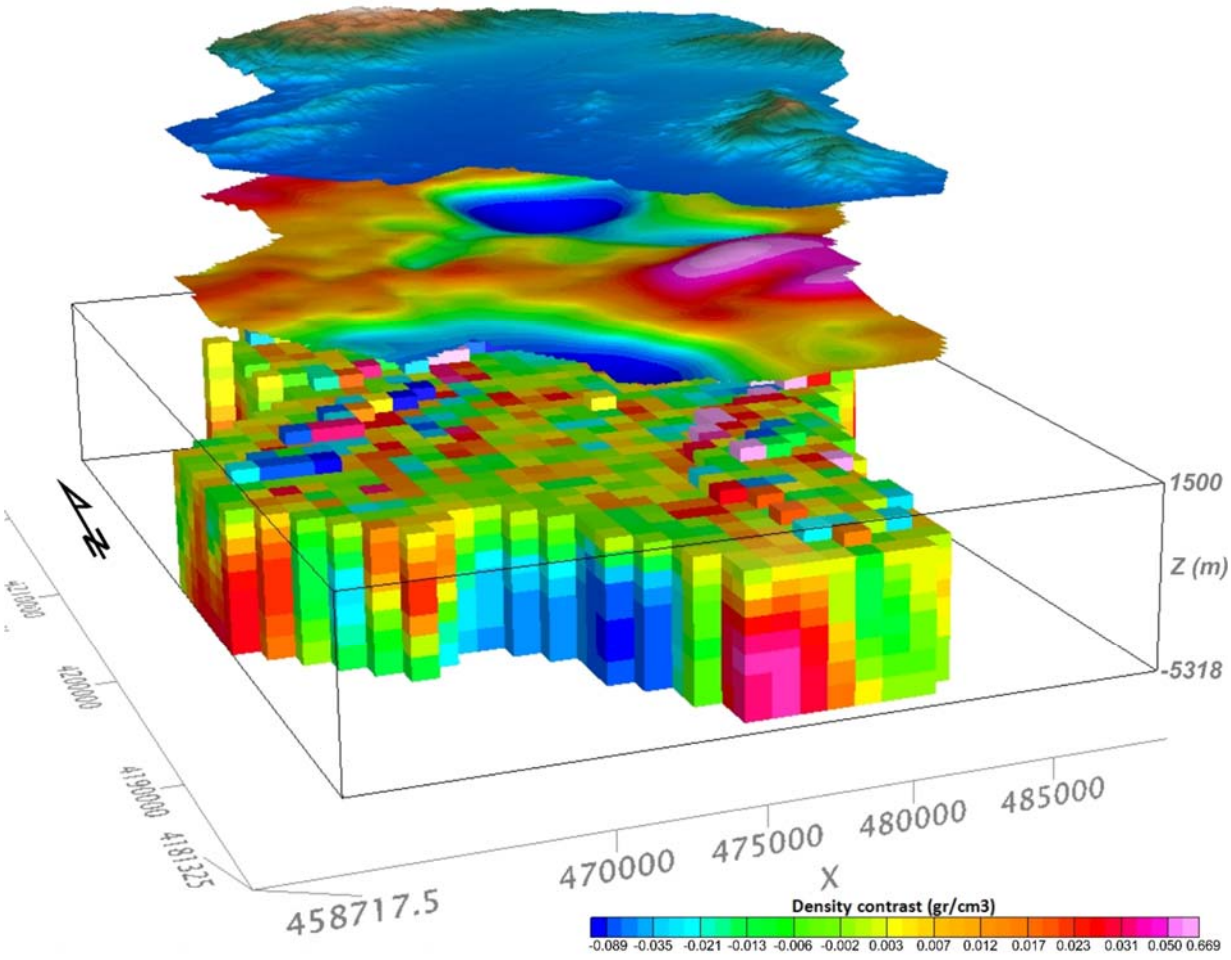


**Figure 7**. 3D gravity inversion of Athens basin, with cell size of 1000 m (mesh 40x29x11 blocks). The area's DEM is presented as the upper plane and is the Residual Anomaly (0.02 cycles/km) as the lower one.

We applied the unconstrained 3D gravity modelling on both Complete Bouguer Anomaly data and the Residual anomaly data in order to compare the results, based on the fact that for the

Complete Bouguer Anomaly, a trend removal procedure has to be first applied. Insignificant differences derived, proving that the trend removal procedure is reliable. The inversion results were almost identical with those of the Residual data, where the regional field has already been removed with the FFT. The desired absolute error was 5%.

We discretized the subsurface in a 3D block mesh, with blocks that have a cell size equal to 1000 meters for X-Y and 500 meters for Z direction (Fig. 7). Therefore, the subsurface area was divided in a total of 12,760 blocks of individual density contrast. The density contrast ranges from -0.32 gr/cm$^3$ (bluish colors) to 0.669 gr/cm$^3$ (reddish colors) for depths up to 6,800 meters (or else absolute elevation -5,300 m). In Figure 8, we provide an alternative pseudo-3D view based on the depth slices (Wang *et al.,* 2011; An and Di, 2016; Bersi *et al.*, 2016; Miller *et al.*, 2017; Andersson and Malehmir, 2018) of the inversion model we have calculated for a better understanding of the subsurface density structure.

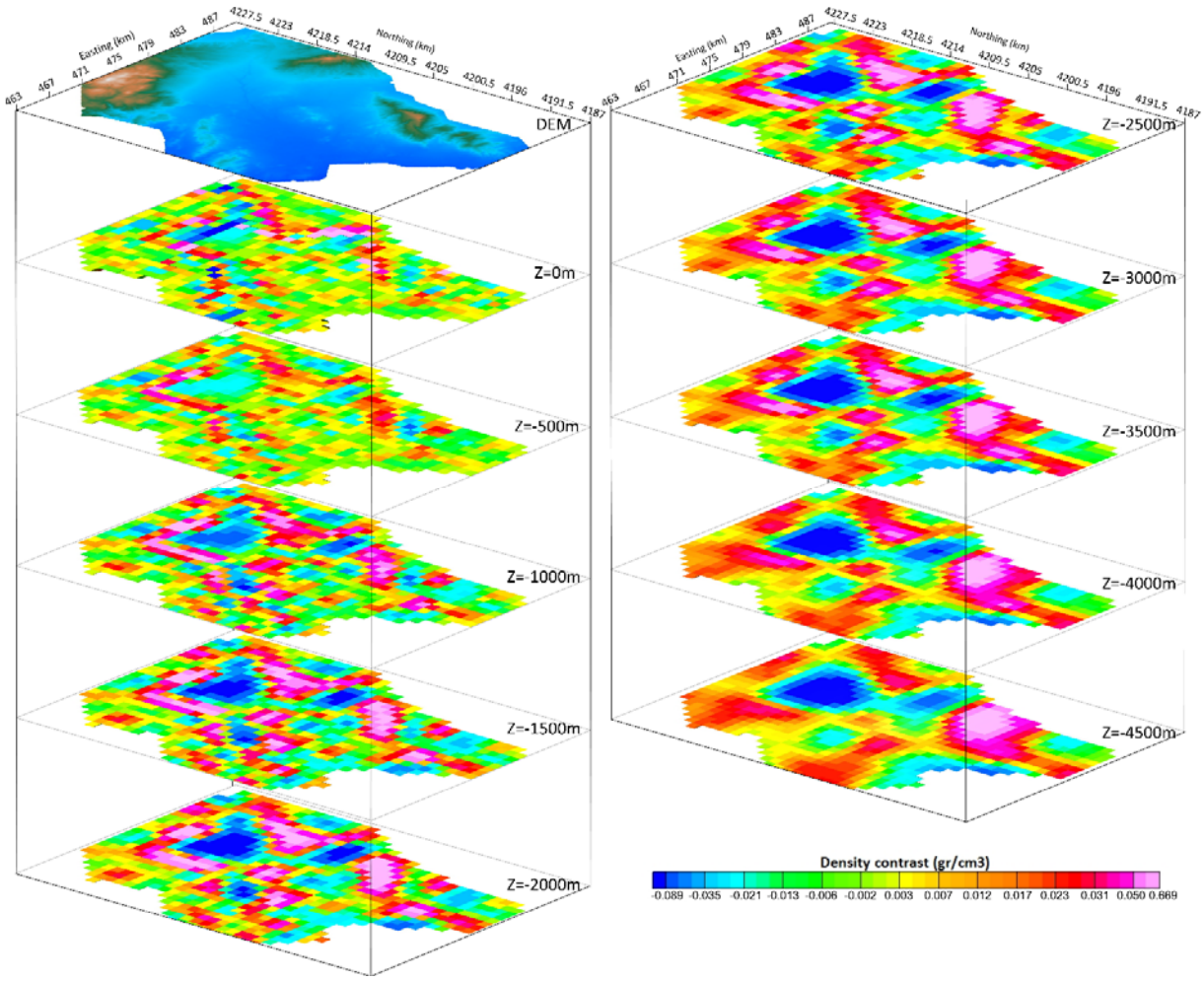


**Figure 8**. Depth slices of the 3D gravity inversion model of Athens basin. The upper left plane illustrates the DEM of the area.

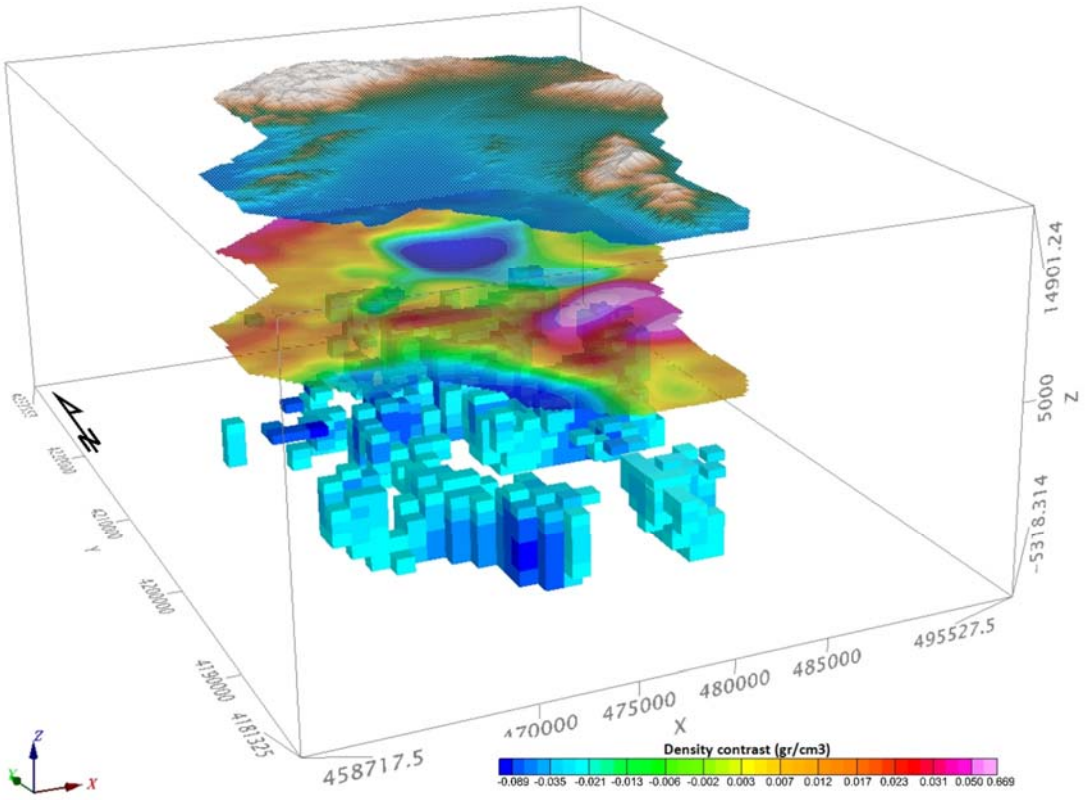


**Figure 9**. 3D gravity inversion results (cell size 1000 m), illustrating the structures of low densities (density contrast from -0.32 to -0.02 gr/cm$^3$).

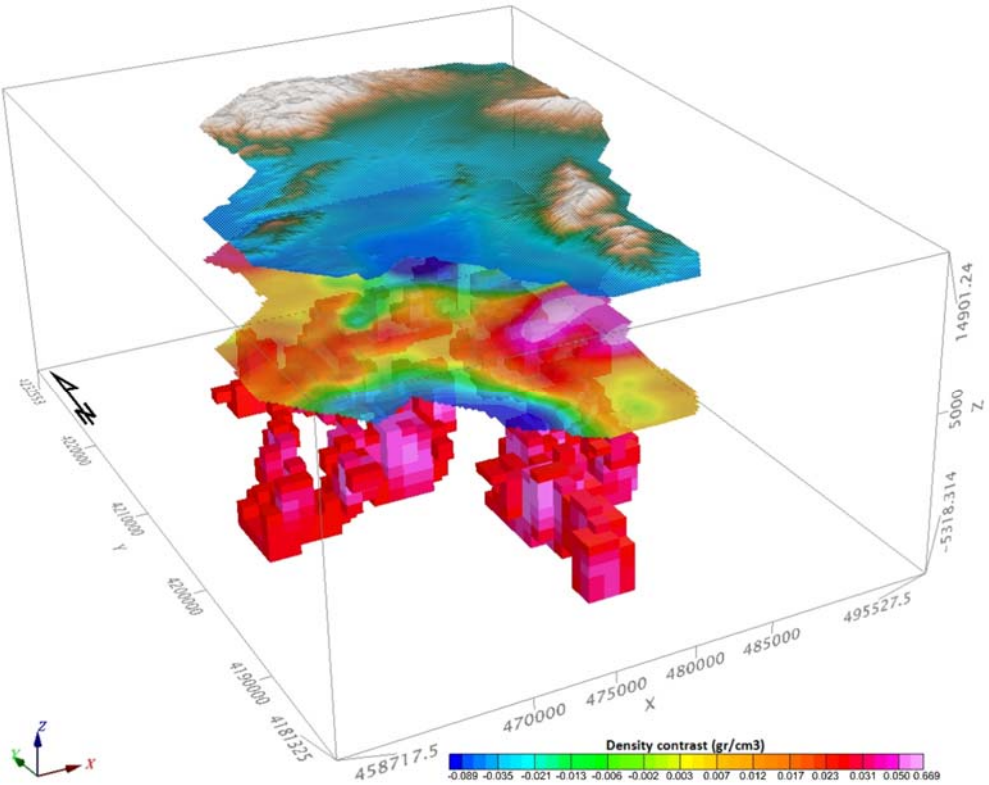


**Figure 10**. 3D gravity inversion results (cell size 1000 m), illustrating the structures of high densities (density contrasts from 0.02 to 0.67 gr/cm$^3$).

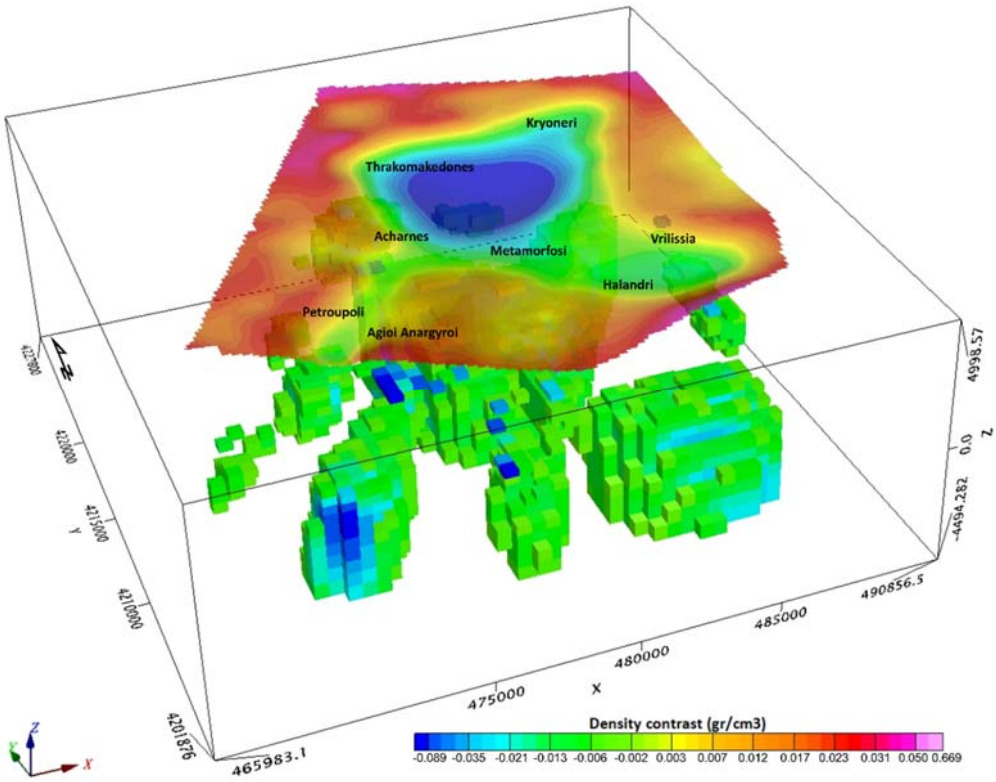


**Figure 11**. 3D gravity model (cell size 500 m, mesh 42x45x17 blocks), showing structures of low densities (density contrast from -0.24 to -0.02 gr/cm$^3$) in the area of *Thrakomakedones, Acharnes, Metamorfosi, Acharnes and Petroupoli.*

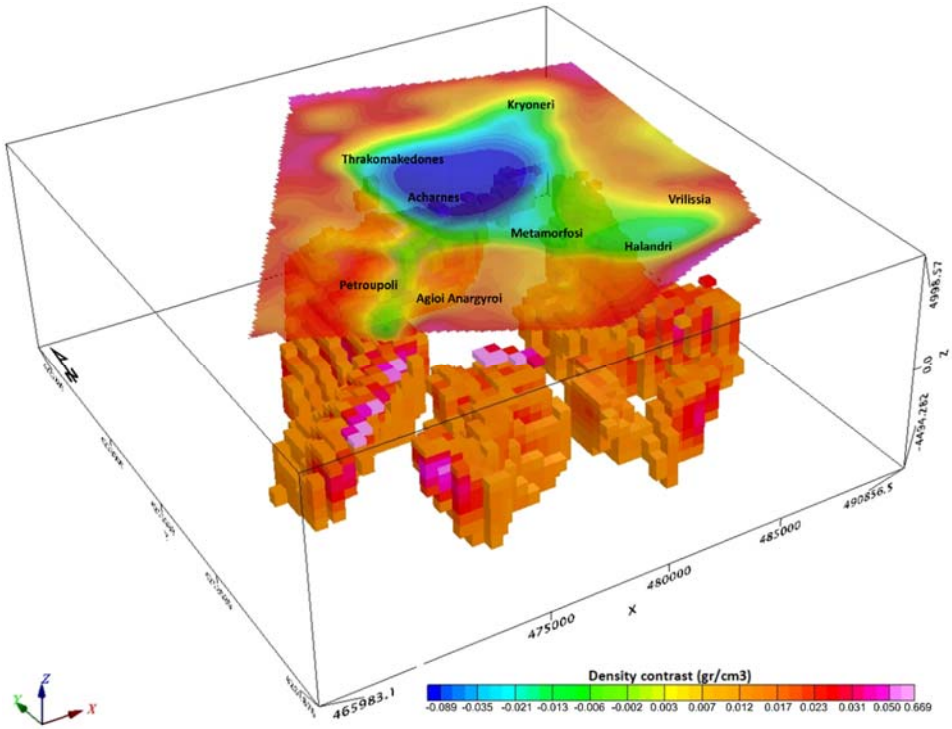


**Figure 12**. 3D gravity model (cell size 500 m, mesh 42x45x17 blocks), showing structures of high densities (density contrast from 0.02 to 0.41 gr/cm$^3$) in the area of *Thrakomakedones, Acharnes, Metamorfosi, Acharnes and Petroupoli*.

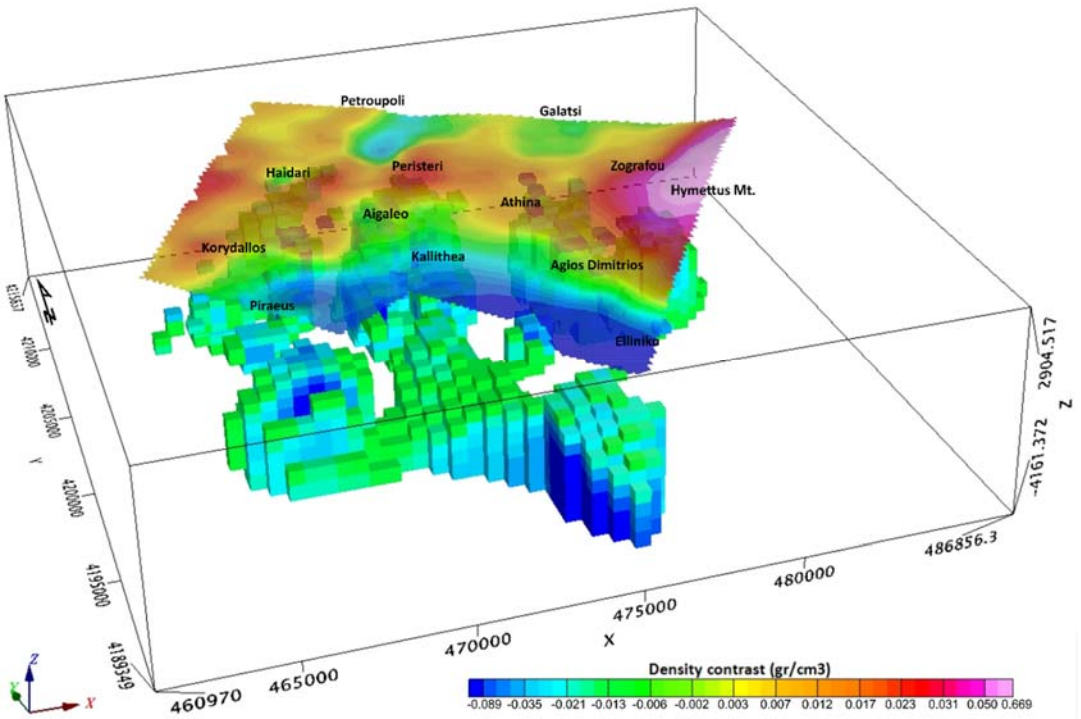


**Figure 13**. 3D gravity model (cell size 500 m, mesh 44x46x13 blocks), showing structures of low densities (density contrast from -0.26 to -0.02 gr/cm$^3$) in the area of *Haidari, Peristeri, Athens and Hymettus Mt.*

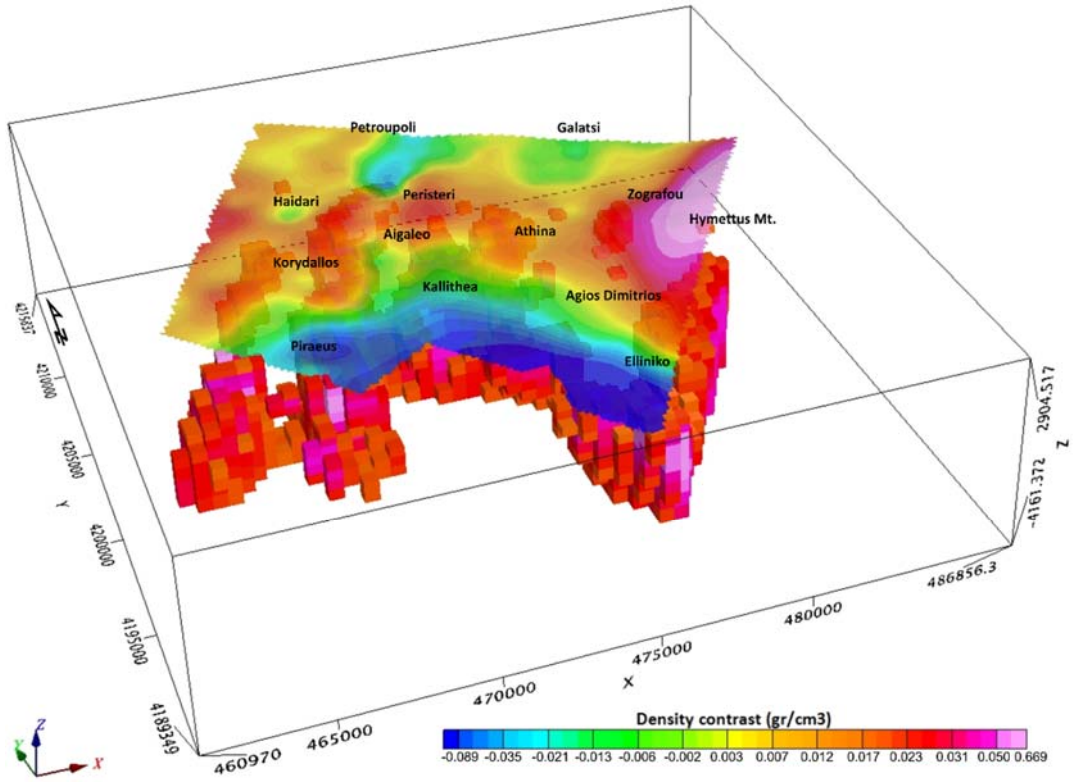


**Figure 14.** 3D gravity model (cell size 500 m, mesh 44x46x13 blocks), showing structures of high densities (density contrast from 0.02 to 0.49 gr/cm$^3$) in the area of *Haidari, Peristeri, Athens and Hymettus Mt.*

In Figure 9, we have isolated the bodies with negative density contrast (ranging from -0.32 to -0.02 gr/cm$^3$) at the areas of *Thrakomakedones, Kryoneri, Drosia, Kifisia, Melissia, Vrilissia, Halandri, Herakleion, Metamorfosi, Acharnes*, *Petroupoli*, *Agioi Anargyroi, Piraeus*, *Palaio Faliro* and *Kalamaki* producing the low gravity anomalies in the Residual maps (Figs. 3-6). In Figure 10, below the areas of Mountains *Hymettus*, *Aigaleo-Poikilo*, *Parnitha* and the *downtown* of Athens city, the bodies with positive density contrast (0.02-0.67 gr/cm$^3$), producing the high gravity anomalies have been adumbrated. These bodies define the geometric boundaries of the anomalies, producing both low and high gravity values respectively. The DEM and the Residual maps have been positioned above the 3D model of the area for a better understanding and evaluation of the results.

Taking into consideration the anomalies already observed in the general model (Figs. 9-10), additional inversions were carried out for smaller areas, in order to reduce the cell size down to 500 meters (Figs. 11-14) or even 250 meters for the horizontal directions. This would provide greater detail of the final 3D density model and consequently better adumbration of the geometry of the source bodies.

The results of the 3D models (Figs. 7-14) are quite impressive and revealed important subsurface structures that might play important role for the seismotectonic structure of Athens basin. Several fault zones already mapped are verified by these models and more information about their characteristics might be gained (e.g. throw, depth and dip). But the most significant contribution of the 3D density models is that they also validate the existence of several fault zones mapped as possible (blind faults), based on other criteria.

### *3.5 2.75D geological-gravity modelling*

Interpretative geological-gravity profiles have been constructed, with the contribution of **GM-SYS** (Leader *et al.,* 2006; Park *et al.,* 2006; Smith *et al*., 2006; Blecha *et al.,* 2009; Kim *et al.,* 2009; Azab and Khadragy, 2013; Blaikie *et al.,* 2014; Weidmann *et al.,* 2016; Ammirati *et al.*, 2018; Dilalos *et al*., 2019a; 2019b). It is a program by *Geosoft* for calculating the gravity response from a geological cross-section, compared to the observed field anomaly response. The models in GM-SYS are built with polygons that represent different geological formations and a density value is assigned at each one. The 2.75D models can have 2D prisms asymmetrically positioned and extended at some distance from the line of the profile, in the strike direction.

In Figure 2, the location of the profiles along the Athens basin, selected to create the interpretative geological-density 2.75-D models, is presented. Two (2) sections have been constructed (Fig. 15) in order to contribute to the adumbration of the tectonic framework of the Athens basin subsurface. The density values assigned to each block/prism are based on the values proposed by Dilalos (2018) and Dilalos *et al.* (2019a). In each of these figures, the upper part illustrates the observed residual gravity data (squares) along with the calculated one (line) based on the geological model, which is illustrated on the lower part of the figures. Each block colored differently, simulates a geological body, with a certain density quoted in the brackets.

303 The sections are presented with a scale 1:2; therefore, there is a vertical exaggeration for better
304 presentation and understanding.

305 ## 4 Discussion

306 In Section CC' (Fig. 15), the Neogene deposits (*Msl*) are observed with thickness, up to 150
307 meters and lateral coverage below the areas of *Agios Ioannis Rentis* and *Tavros*, producing the
308 low residual values (down to -1 mGal). There is also a layer of 40-50 meters of Alluvium
309 deposits (*Al*) and Pleistocene Talus and Screes (*Pt.sc*), overlying. Between the areas of
310 *Korydallos* and *Tavros,* a few **neotectonic fault zones** have been discovered beneath the
311 Neogene deposits and their underlying formation of Athens Schists. A great part of the
312 subsurface, beneath the Neogene deposits, is covered by the Athens Schists (*SchA*) and the
313 Schists of Alepovouni Unit (*Sch-Al*), with a maximum thickness of 300 and 155 meters
314 correspondingly. Furthermore, the Dolomites (*D*) of the *Metamorphic Unit* seem to dominate at
315 the lower area below the basin (from depths of 350 meters) and the *Hymettus Mountain*, with
316 thickness that reaches 950 meters. The Marbles (*M*) are also detected below *Hymettus Mountain*,
317 while the Schists (*Sch*) have been restrained to a thin layer of a few meters. A structure similar to
318 the one of **extension-parallel folds** (Avigad *et al*., 2001; Levy and Jaupart, 2011; Le Pourhiet *et*
319 *al*., 2012) seems to appear among the formation of the *Metamorphic Unit*. The formation of
320 Varis Schists (*Sch Vari*) is also illustrated underlying the Dolomites (*D*) at the end of the section.

321 In Section EE' (Fig. 15), the Neogene deposits are observed below the areas of *Piraeus* (*Plm*)
322 and *Marousi* (*Pll*), with thickness, up to 250 and 200 meters correspondingly, producing the low
323 values in the residual gravity field (down to -4.8 mGal). At the area of *Piraeus* and *Neo Faliro* a
324 couple of **neotectonic fault zones** have been revealed at the basement of the post-alpine
325 deposits. There is also a layer of 40-50 meters of Alluvium deposits (*Al*) partially overlying the
326 Plm sediments at *Piraeus* area. The first part of the section is dominated by the existence of the
327 Triassic-Jurassic Limestones (*T-J*). The Athens Schists (*SchA*), with great surface exposure
328 (outcrops), also cover a great part of the subsurface, with maximum thickness up to 600 meters,
329 mostly below the central area of the basin. The Schists of *Alepovouni Unit* (*Sch-Al*) have been
330 determined with a thin layer of maximum thickness of 200 meters, below the Athens Schists. At
331 the central area of the profile (from depths of 300 meters) and below the *Penteli Mountain*, the
332 Dolomites (*D*) of the *Metamorphic Unit* seem to dominate, with thickness that reaches 750
333 meters. The Schists (*Sch*) seem to dominate against the Marbles (*M*) below *Penteli Mountain,*
334 since they appear with thicknesses up to 1,750 and 100 meters correspondingly.

335 There are some common major fault zones that have been delineated along both sections. The
336 **West Cycladic Detachment System** (Iglseder *et al*., 2011; Lekkas *et al*., 2011; Grasemann *et*
337 *al*., 2012; Seman *et al*., 2012; 2013; Coleman *et al*., 2018) seems to have been identified, along
338 which the underlying metamorphosed *Metamorphic Unit* is moving upwards relatively to the
339 overlying tectonic units of *Ypopelagoniki, Athens* and *Alepovouni*. The schists of *Alepovouni*
340 *Unit* (*Sch-Al*) or the Athens Schists (*SchA*) are mostly located overlying. The dolomites (*D*),
341 schists (*Sch*) or even the marbles (*M*) of the *Metamorphic Unit* are located underlying.

Furthermore, three to four **upthrusts** between the Triassic-Jurassic limestones (*T-J*) and the Shales and Sandstones alterations (*C-P*) seem to have been recognized. Beyond that, a **thrust fault** with the Athens Schists (*SchA*) of the *Athens Unit* overlaying tectonically on the *Ypopelagoniki Unit* can also be observed along both sections.

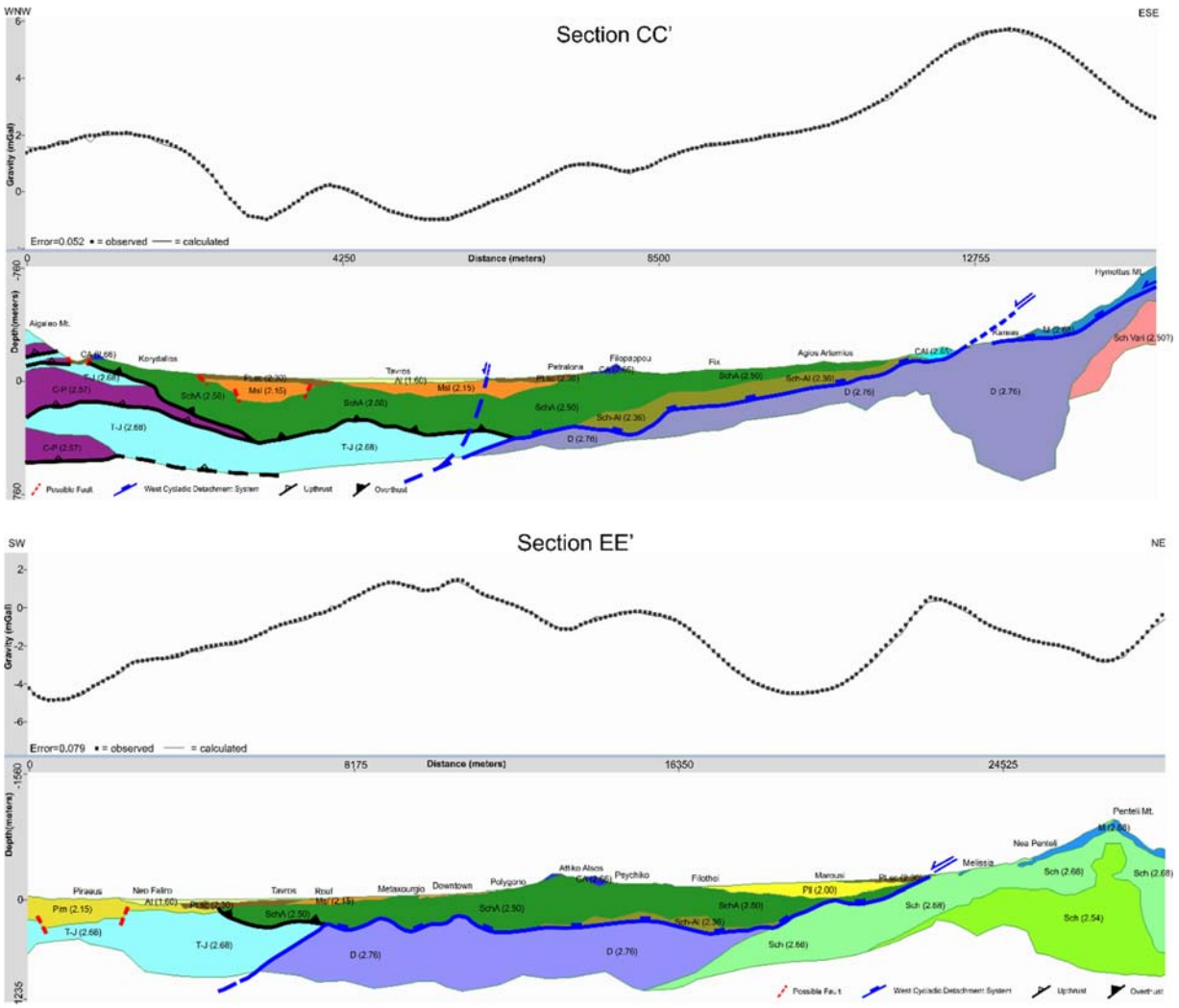


**Figure 15.** Interpretative geological 2.75-D profiles (scale 1:2). The observed (squares) and calculated (line) residual anomaly are illustrated. The geological formations are:

**T-J:** Triassic-Jurassic Limestones (*Ypopelagoniki Unit*), **C-P**: Shales and Sandstones alterations (*Ypopelagoniki Unit*), **M:** Marbles (*Metamorphic Unit*), **Sch:** Schists (*Metamorphic Unit*), **D:** Dolomites (*Metamorphic Unit*), **Sch-Vari:** Varis Schists (*Metamorphic Unit*), **SchA:** Athens Schists (*Athens Unit*); **CA:** Limestones (*Athens Unit*), **Sch-Al:** Schists (*Alepovouni Unit*), **CAl:** Limestones (*Alepovouni Unit*), **Msl:** Upper Miocene Terrestrial and Lacustrine deposits (*Neogene Formations*), **Pt.sc:** Pleistocene Talus and Screes, **Al:** Alluvium deposits (*Loose Quaternary deposits).*

## 5 Conclusions

In this paper, the quantitative results of an urban gravity survey of Athens city basin have been presented. More specifically, a total of 1,120 gravity measurements were acquired, based on a grid plan and supported by a newly established gravity base network. Due to the difficulties raised from the urban characteristics of the area, the acquisition planning was organized very carefully. Beyond that, during the standard reduction processing, an additional Building Correction has been added in order to remove the gravitational effect of the buildings on the measurements.

The next step involves the application of the Euler deconvolution in order to calculate depth solutions for the residual maps of the area. Two different techniques have been applied, the *Standard Euler* and the *Located* one but also two different Structural Indexes (0 and 1). At first, it seems that the *Standard Euler* method (Figs. 3-4) provides better results and far more solutions than the *Located* one (Figs. 5-6). One the other hand, the Structural Index 0 (Figs. 3 & 5) produces less solutions than the Structural Index 1 (Figs. 4 & 6). Additionally, the Euler deconvolution depth solutions (Figs. 3-6), for both selected Structural Indexes (0 and 1) and for both applied Euler deconvolution methods (*Standard* and *Located*), seem to have great similarities to the structural maps presented by Dilalos (2018) and Dilalos *et al*. (2019a). The calculated depths are ranging close to the source depths that have been estimated by the Energy Spectrum Analysis, except for some solutions of SI=1 that reach greater depths. Based on these maps, we managed to retrieve quantitative information for the depths of anomalous sources, ranging between 500 and 3,760 meters.

Furthermore, the unconstrained 3D density model of the area has been constructed (Figs. 7-8) in order to obtain a good image of the density distribution of the subsurface. The model information reaches the depth of 4,500 meters, which is considered quite important for the area. For a better understanding of the 3D density distribution and in an effort to delineate better the tectonic structures, we selected to present it in two separate images; one illustrating only the structures of lower densities and one other only with the structures of higher densities (Figs. 9-14). Figures 9-10 present the whole study area, while Figures 11-14 present two focused areas in detail.

Finally, two geophysical-geological profiles (Fig. 15) have been constructed and presented. Practically, along with these two sections we present the geological interpretation of the gravity survey, providing valuable new information for the geotectonic regime of the subsurface. Along with these sections several geotectonic structures have been adumbrated, such as neotectonics fault zones, upthrusts, thrust fault, extension-parallel folds and a structure evaluated as the West Cycladic Detachment System. Beyond these, the thickness of several geological formations has also been estimated. For example, the Neogene deposits appear with 250 meters maximum thickness, the Athens Schists (*SchA*) with 600 meters and the schists of *Alepovouni Unit* (*Sch-Al*) with 200 meters. Additionally, the Dolomites (*D*) and the Schists (*Sch*) appear with thickness 950 and 1,750 meters correspondingly.

The 2.75D interpretative profiles and the 3D density models revealed important subsurface structures for the geotectonic structure of Athens basin subsurface, for depths up to 2,500 meters. Several fault zones already mapped are verified by these models (Dilalos, 2018; Dilalos *et al.*; 2019a) and more information about their characteristics might be gained (e.g. throw, depth and dip). But the most significant contribution is that, along with the Euler deconvolution depths, they also validate the existence of several fault zones mapped as possible (blind faults), based on other criteria. The 3D density models (Figs. 7-14) define in a good way the geometry of the identified anomaly bodies and therefore the geometry of the subsurface geology.

## 6 Acknowledgments

We would like to thank Dr. Stylianos Lozios for his geological advice and important guidance during the interpretation of the data. Additionally, we would like to thank Mr. Stylianos Chailas for the provision of the data for the existing gravity base in the University of Athens. The authors would also like to thank Ms. Achtypi S., Ms. Kaplanidi H., Mr. Papaelias S., Mr. Mavroulis S., Dr. Michelioudakis D. and Ms. Drosopoulou E. for their valuable contribution to the field measurements.

## 7 Declarations

### Funding

The fieldwork was supported by the Special Account for Research Grants of the UoA (contract no. 70/4/9254)

### Conflicts of interest/Competing interests

None

### Availability of data and material

Data will be made available on request

## 8 References

Ammirati J.B., Venerdini A., Alcacer J.M., Alvarado P., Miranda S., Gilbert H. (2018) New insights on regional tectonics and basement composition beneath the eastern Sierras Pampeanas (Argentine back-arc region) from seismological and gravity data. *Tectonophysics* 740:42-52. https://doi.org/10.1016/j.tecto.2018.05.015

An Z., Di Q. (2016) Investigation of geological structures with a view to HLRW disposal, as revealed through 3D inversion of aeromagnetic and gravity data and the results of CSAMT exploration. *Journal of Applied Geophysics* 135:204-211. https://doi.org/10.1016/j.jappgeo.2016.10.013

Andersson M., Malehmir A. (2018) Internal architecture of the Alnö alkaline and carbonatite complex (central Sweden) revealed using 3D models of gravity and magnetic data. *Tectonophysics* 740-741:53-71. https://doi.org/10.1016/j.tecto.2018.05.008

Anudu G.K., Stephenson R.A., Macdonald D.I., Oakey G.N. (2016) Geological features of the northeastern Canadian Arctic margin revealed from analysis of potential field data. *Tectonophysics* 691:48-64. https://doi.org/10.1016/j.tecto.2016.03.025

Avigad, D. Ziv, A. Garfunkel, Z. (2001) Ductile and brittle shortening, extension-parallel folds and maintenance of crustal thickness in the central Aegean (Cyclades, Greece). *Tectonics* 20(2):277-287. https://doi.org/10.1029/2000TC001190

Azab A.A., El-Khadragy A.A. (2013) 2.5-D Gravity/Magnetic Model Studies in Sahl El Qaa Area, Southwestern Sinai, Egypt. *Pure and Applied Geophysics* 170(12):2207-2229. https://doi.org/10.1007/s00024-013-0650-5

Azizi M., Saibi, H. (2015) Integrating gravity data with remotely sensed data for structural investigation of the Aynak-Logar Valley, eastern Afghanistan, and the surrounding area. IEEE *Journal of Selected Topics in Applied Earth Observations and Remote Sensing* 8(2):816-824. Doi: 10.1109/JSTARS.2014.2347375

Berg J.W., Thiruvathukal J.V. (1965) Gravity base station network, Oregon. *Journal of Geophysical Research* 70(14):3325-3330. Doi: 10.1029/JZ070i014p03325

Bersi, M. Saibi, H. Chabou, M.C. (2016) Aerogravity and remote sensing observations of an iron deposit in Gara Djebilet, southwestern Algeria. *Journal of African Earth Sciences* 116:134-150. https://doi.org/10.1016/j.jafrearsci.2016.01.004

Blaikie T.N., Ailleres L., Betts P.G., Cas R.A.F. (2014) Interpreting subsurface volcanic structures using geologically constrained 3-D gravity inversions: examples of maar-diatremes, Newer Volcanics Province, southeastern Australia. J*ournal of Geophysical Research: Solid Earth* 119(4):3857-3878. Doi: 10.1002/2013JB010751

Blecha V., Štemprok, M. Fischer, T. (2009) Geological interpretation of gravity profiles through the Karlovy Vary granite massif (Czech Republic). *Studia Geophysica et Geodaetica* 53(3):295-314. https://doi.org/10.1007/s11200-009-0019-5

Boszczuk P., Cheng L.Z., Hammouche H., Roy P., Lacroix S., Cheilletz A. (2011) A 3D gravity data interpretation of the Matagami mining camp, Abitibi Subprovince, Superior Province, Québec, Canada: Application to VMS deposit exploration. *Journal of Applied Geophysics* 75(1):77-86. https://doi.org/10.1016/j.jappgeo.2011.06.031

Casten U., Snopek K. (2006) Gravity modelling of the Hellenic subduction zone - A regional study. *Tectonophysics* 417(3-4):183-200. https://doi.org/10.1016/j.tecto.2005.11.002

Choi S., Götze H.J., Meyer U., DESIRE Group (2011) 3-D density modelling of underground structures and spatial distribution of salt diapirism in the Dead Sea Basin. *Geophysical Journal International* 184(3):1131-1146. https://doi.org/10.1111/j.1365-246X.2011.04939.x

Coleman M., Soukis K., Schnider D., Grasemann B., Lozios S. (2018) The northwest termination of the West Cy-cladic Detachment System in Central Attica. In: *EGU General Assembly Conference Abstracts* 20:5172.

Commer M. (2011) Three-dimensional gravity modelling and focusing inversion using rectangular meshes. *Geophysical Prospecting* 59(5):966-979. Doi: 10.1111/j.1365-2478.2011.00969.x

Csapó G., Völgyesi L. (2002) Hungary's new gravity base network (MGH-2000) and it's connection to the European unified gravity net. In: *Vistas for Geodesy in the New Millennium*, 72-77. Springer, Berlin, Heidelberg.

Curto J.B., Vidotti R.M., Blakely R.J., Fuck R.A. (2015) Crustal framework of the northwest Paraná Basin, Brazil: Insights from joint modeling of magnetic and gravity data. *Tectonophysics* 655:58-72. http://dx.doi.org/10.1016/j.tecto.2015.05.011

Damaceno J.G., de Castro D.L., Valcácio S.N., Souza Z.S. (2017) Magnetic and gravity modeling of a Paleogene diabase plug in Northeast Brazil. *Journal of Applied Geophysics* 136:219-230. https://doi.org/10.1016/j.jappgeo.2016.11.006

de Castro D.L., Fuck R.A., Phillips J.D., Vidotti R.M., Bezerra F.H., Dantas E.L. (2014) Crustal structure beneath the Paleozoic Parnaíba Basin revealed by airborne gravity and magnetic data, Brazil. *Tectonophysics* 614:128-145. https://doi.org/10.1016/j.tecto.2013.12.009

Dilalos S. (2018) Application of geophysical technique to the investigation of tectonic structures in urban and suburban environments. A case study in Athens basin. ***Ph.D. Thesis*** National and Kapodistrian University of Athens.

Dilalos S., Alexopoulos J.D. (2017) Indications of correlation between gravity measurements and isoseismal maps. A case study of Athens basin (Greece). *Journal of Applied Geophysics* 140:62-74. https://doi.org/10.1016/j.jappgeo.2017.03.012

Dilalos S., Alexopoulos J.D. (2019a) Urban Gravity Measurements for the Subsurface Investigation of Athens Basin (Greece). *Bulletin of the Geological Society of Greece* Special Publication 7: 211-212.

Dilalos S., Alexopoulos J.D. (2019b) Quantitative subsurface information of Athens basin (Greece) derived from urban gravity measurements. In: *Near Surface Geoscience 2019-1st Conference on Geophysics for Infrastructure Planning Monitoring and BIM*: We_INFRA_P23. Doi: 10.3997/2214-4609.201902560

Dilalos S., Alexopoulos J.D., Lozios S. (2019a) New insights on Athens basin (Greece) subsurface geological and tectonic structure, derived from urban gravity measurements. *Journal of Applied Geophysics* 167(C):73-105. https://doi.org/10.1016/j.jappgeo.2019.04.024

Dilalos S., Alexopoulos J.D., Lozios S. (2019b) The contribution of urban gravity survey to the subsurface geological structure of the Athens basin (Greece). In: *Near Surface Geoscience 2019-25th European Meeting of Environmental and Engineering Geophysics*: We_25_P17. Doi: 10.3997/2214-4609.201902472

Dilalos S., Alexopoulos J.D., Tsatsaris A. (2018) Calculation of Building Correction for urban gravity surveys. A case study of Athens metropolis (Greece). *Journal of Applied Geophysics* 159(C):540-552. https://doi.org/10.1016/j.jappgeo.2018.09.036

European Environment Agency (2012) CORINE Land Cover Project.

Farhi W., Boudella A., Saibi H., Bounif M.O.A. (2016) Integration of magnetic, gravity, and well data in imaging subsurface geology in the Ksar Hirane region (Laghouat, Algeria). *Journal of African Earth Sciences* 124:63-74. https://doi.org/10.1016/j.jafrearsci.2016.09.013

Fernandez-Cordoba J., Zamora-Camacho A., Espindola J.M. (2017) Gravity Survey at the Ceboruco Volcano Area (Nayarit, Mexico): A 3-D Model of the Subsurface Structure. *Pure and Applied Geophysics* 174(10): 3905-3918. https://doi.org/10.1007/s00024-017-1600-4

FitzGerald D., Reid A., McInerney P. (2004) New discrimination techniques for Euler deconvolution. *Computers & Geosciences* 30(5):461-469. https://doi.org/10.1016/j.cageo.2004.03.006

Freyberg B.V. (1951) Das Neogen-Gebiet nordwestlich Athen. *Annales Géologiques des Pays Helléniques* 3:65–86 (*In German*)

Grasemann B., Schneider D., Stöckli D., Iglseder C. (2012) Miocene bivergent crustal extension: evidence from the western Cyclades (Greece). *Lithosphere* 4 (1):23–39. Doi: 10:1130/L164.1

Hipkin R.G., Lagios E., Lyness D., Jones P. (1988) Reference gravity stations on the IGSN71 standard in Britain and Greece. *Geophysical Journal International* 92(1):143-148. https://doi.org/10.1111/j.1365-246X.1988.tb01128.x

Hosseini A.A., Doulati Ardejani F., Tabatabaie S.H., Hezarkhani A. (2013) Edge detection in gravity field of the Gheshm sedimentary basin. *International Journal of Mining & Geo-Engineering* 47(1):41-50. Doi: 10.22059/IJMGE.2013.50089

Iglseder C., Grasemann B., Rice A.H.N., Petrakakis K., Schneider D.A. (2011) Miocene south directed low-angle normal fault evolution on Kea Island (West Cycladic Detachment System, Greece). *Tectonics* 30(4): 1-31. Doi: 10.1029/2010TC002802

Katsikatsos G. (1977) La structure tectonique d'Attique et de l'île d'Eubée. In: *Proceedings of the 6th Colloquium of the Geology of the Aegean Region* 1: 211-228, IGME publications (*In French*).

Katsikatsos G., Migiros G., Triantaphyllis M., Mettos A. (1986) Geological structure of internal Hellenides (E.Thessaly–SW Macedonia–Euboea–Attica–Northern Cyclades islands and Lesvos). *Geological and Geophysical Research* Special Issue:191-212. IGME publications.

Keating P.B. (1998) Weighted Euler deconvolution of gravity data. *Geophysics* 63(5):1595-1603. https://doi.org/10.1190/1.1444456

Khalil M.A., Santos F.M., Farzamian M. (2014) 3D gravity inversion and Euler deconvolution to delineate the hydro-tectonic regime in El-Arish area, northern Sinai Peninsula. *Journal of Applied Geophysics* 103:104-113. https://doi.org/10.1016/j.jappgeo.2014.01.012

Khamies A.A., El-Tarras M.M. (2010) Surface and subsurface structures of Kalabsha area, southern Egypt, from remote sensing, aeromagnetic and gravity data. *The Egyptian Journal of Remote Sensing and Space Science* 13(1):43-52. https://doi.org/10.1016/j.ejrs.2010.07.006

Kim Y.M., Lee S.M., Okino K. (2009) Comparison of gravity anomaly between mature and immature intra-oceanic subduction zones in the western Pacific. *Tectonophysics* 474(3-4):657-673. https://doi.org/10.1016/j.tecto.2009.05.004

Koumetio F., Njomo D., Tabod C.T., Noutchogwe T.C., Manguelle-Dicoum E. (2012) Structural interpretation of gravity anomalies from the Kribi–Edea zone, South Cameroon: A case study. *Journal of Geophysics and Engineering* 9(6):664. Doi: 10.1088/1742-2132/9/6/664

Krohe A., Mposkos E., Diamantopoulos A., Kaouras G. (2010) Formation of basins and mountain ranges in Attica (Greece): The role of Miocene to Recent low-angle normal detachment faults. *Earth-Science Reviews* 98(1-2):81–104.

https://doi.org/10.1016/j.earscirev.2009.10.005
Krynski J., Olszak T., Barlik M., Dykowski P. (2013) New gravity control in Poland–needs, the concept and the design. *Geodesy and Cartography* 62(1):3-21. https://doi.org/10.2478/geocart-2013-0001
Lagios E. (1985) A gravity network in central Greece for secular gravity studies. *Pure and Applied Geophysics* 123(1):81-90. https://doi.org/10.1007/BF00877050
Le Pourhiet L., Huet B., May D.A., Labrousse L., Jolivet L. (2012) Kinematic interpretation of the 3D shapes of metamorphic core complexes. *Geochemistry, Geophysics, Geosystems* 13(9): Q09002. Doi: 10.1029/2012GC004271.
Leader L.D., Rawling T.J., Wilson C.J.L. (2006) Structural transect and forward modelling of geophysical data across the St Arnaud Group, Victoria. *Australian Journal of Earth Sciences* 53(5):863-873. https://doi.org/10.1080/08120090600827504
Lekkas S., Lozios S. (2000) Tectonic structure of Mt. Hymittos. *Annales Géologiques des Pays Helléniques* 38: 47-62.
Lekkas S., Skourtsos E., Soukis K., Kranis H., Lozios S., Alexopoulos A., Koutsovitis P. (2011) Late Miocene detachment faulting and crustal extension in SE Attica (Greece). *Geophysical Research Abstracts* 13:EGU2011-13016.
Lepsius R. (1893) Geologie von Attika. Ein Beitrag zur Lehre von Metamorphismus der *Gesteine, Berlin Zeitschr. f. prakt. Geol*. 4 196S: 592p. (*In German*).
Levy F., Jaupart C. (2011) Folding in regions of extension. *Geophysical Journal International* 185(3):1120–1134. https://doi.org/10.1111/j.1365-246X.2011.05013.x
Lozios S. (1993) Tectonic analysis of the metamorphic formations of NE Attica. *PhD Thesis*, National and Kapodistrian University of Athens (*In Greek*) http://hdl.handle.net/10442/hedi/2925
Makris J., Papoulia J., Yegorova T. (2013) A 3-D density model of Greece constrained by gravity and seismic data. *Geophysical Journal International* 194(1):1-17. https://doi.org/10.1093/gji/ggt059
Marinos G., Katsikatsos G., Georgiadou-Dikeoulia E., Mirkou E. (1971) The Athens' schist formation I. Stratigraphy and Structure. *Annales Géologiques des Pays Helléniques* 23:183-212 (*In Greek*).
Marinos G., Katsikatsos G., Mirkou E. (1974) The Athens' schist formation II. Stratigraphy and Structure. *Annales Géologiques des Pays Helléniques* 25:439-444 (*In Greek*)
Mariolakos I., Fountoulis I., Mariolakos D., Andreadakis E., Georgakopoulos A. (2000) Geodynamic phenomena observed during the Athens earthquake (Ms= 5.9) 7-9-1999. *Annales Géologiques des Pays Helléniques* 38:175-186.
Martinez C., Li Y., Krahenbuhl R., Braga M.A. (2013) 3D inversion of airborne gravity gradiometry data in mineral exploration: A case study in the Quadrilátero Ferrífero, Brazil. *Geophysics* 78(1):B1-B11. Doi: 10.1190/geo2012-0106.1
Martins-Ferreira M.A.C., Campos J.E.G., Von Huelsen M.G., Neri B.L. (2018) Paleorift structure constrained by gravity and stratigraphic data: The Statherian Araí rift case. *Tectonophysics* 738-739:64-82. https://doi.org/10.1016/j.tecto.2018.05.014
Miller C.A., Williams-Jones G., Fournier D., Witter J. (2017) 3D gravity inversion and thermodynamic modelling reveal properties of shallow silicic magma reservoir beneath Laguna

582 del Maule, Chile. *Earth and Planetary Science Letters* 459:14-27.
583 https://doi.org/10.1016/j.epsl.2016.11.007
584 Morelli C., Gantar C., Honkasalon T., McConnel K., Tanner J.G., Szabo B., Uotila U., Whalen
585 C.T. (1974) *The International Standardization Net 1971 (IGSN71)*. IUGG-IAG Publ. Spec. 4.
586 Int. Union of Geod. and Geophysics.
587 Naouali B.S., Inoubli M.H., Amiri A., Chaqui A., Hamdi I. (2011) Subsurface geology of the
588 Ariana region (Diapir Zone, northern Tunisia) by means of gravity analysis. *Geophysical*
589 *Prospecting* 59(6):983-997. Doi: 10.1111/j.1365-2478.2011.01004.x
590 Nasr I.H., Amiri A., Inoubli M.H., Salem A.B., Chaqui A., Tlig S. (2011) Structural setting of
591 northern Tunisia insights from gravity data analysis Jendouba case study. *Pure and Applied*
592 *Geophysics* 168(10):1835-1849. https://doi.org/10.1007/s00024-010-0189-7
593 Niedermayer J. (1971) Die geologische Karte von Athen 1:10.000. *Bulletin of the Geological*
594 *Society of Greece* 8(2):117-134 (*In German*).
595 Papadopoulos T.D., Goulty N., Voulgaris N.S., Alexopoulos J.D., Fountoulis I., Kambouris P.,
596 Karastathis V., Peirce C., Chailas S., Kassaras J., Pirli M. (2007) Tectonic structure of Central-
597 Western Attica (Greece) based on geophysical investigations-preliminary results. *Bulletin of the*
598 *Geological Society of Greece* 40(3):1207-1218.
599 Papanikolaou D. (1986). *Geology of Greece*. Heptalofos, Athens (*In Greek*).
600 Papanikolaou D., Lozios S., Sideris C., Kranis H., Danamos G., Soukis K., Skourtsos E., Bassi
601 E., Marinos P., Tsiampaos G., Boukovalas G., Sabatakakis N., Antoniou A., Provia K. (2002)
602 Geological-Geotechnical study of Athens basin. *OASP Applied research program*, Athens (*In*
603 *Greek*).
604 Papanikolaou D.I., Lozios S.G., Soukis K., Skourtsos E. (2004) The geological structure of the
605 allochthonous '*Athens Schists'*. *Bulletin of the Geological Society of Greece* 36(4):1550-1559 (*In*
606 *Greek*).
607 Park C.H., Kim J.W., Isezaki N., Roman D.R., von Frese R.R. (2006) Crustal analysis of the
608 Ulleung Basin in the East Sea (Japan Sea) from enhanced gravity mapping. *Marine Geophysical*
609 *Researches* 27(4):253-266. Doi: 10.1007/s11001-006-9006-1
610 Prutkin I., Vajda P., Tenzer R., Bielik M. (2011) 3D inversion of gravity data by separation of
611 sources and the method of local corrections: Kolarovo gravity high case study. *Journal of*
612 *Applied Geophysics* 75(3):472-478. https://doi.org/10.1016/j.jappgeo.2011.08.012
613 Reid A.B., Ebbing J., Webb S.J. (2012) Comment on 'A crustal thickness map of Africa derived
614 from a global gravity field model using Euler deconvolution'by Getachew E. Tedla, M. van der
615 Meijde, AA Nyblade and FD van der Meer. *Geophysical Journal International* 189(3):1217-
616 1222. https://doi.org/10.1111/j.1365-246X.2012.05353.x
617 Reid A.B., Ebbing J., Webb S.J. (2014a) Avoidable Euler errors–the use and abuse of Euler
618 deconvolution applied to potential fields. *Geophysical Prospecting* 62(5):1162-1168. Doi:
619 10.1111/1365-2478.12119
620 Reid A.B., Thurston J.B. (2014b) The structural index in gravity and magnetic interpretation:
621 Errors, uses, and abuses. *Geophysics* 79(4):J61-J66. https://doi.org/10.1190/geo2013-0235.1

Robertson E.I., (1965) Gravity base stations in the south-west Pacific Ocean. *New Zealand Journal of Geology and Geophysics* 8(3):424-439. https://doi.org/10.1080/00288306.1965.10426414

Sabatakakis N. (1991) Engineering geological setting of Athens basin. *PhD Thesis* University of Patras (*In Greek*) http://hdl.handle.net/10442/hedi/1734

Seman S., Soukis K., Stockli D.F., Skourtsos E., Kranis H., Lozios S. (2012) Novel Thermochrono-metric Techniques Applied to the Lavrion Detachment, Lavrion Peninsula, Attica, Greece. *Mineralogical Magazine*, *Abstracts* 76:2352.

Seman S., Soukis K., Stockli D.F., Skourtsos E., Kranis H., Lozios S. (2013) Provenance of metasediments and Miocene exhumation history of the Lavrion Peninsula, South Attica, Greece: a combined structural, (U-Th)/He, and detrital zircon U-Pb study. *Geophysical Research Abstracts* 15:EGU2013-12605.

Slack H.A., Lynch V.M., Langan L. (1967) The geomagnetic gradiometer. *Geophysics* 32(5):877-892. https://doi.org/10.1190/1.1439897

Smith N., Cassidy J., Locke C.A., Mauk J.L., Christie A.B. (2006) The role of regional-scale faults in controlling a trapdoor caldera, Coromandel Peninsula, New Zealand. *Journal of Volcanology and Geothermal Research* 149(3-4):312-328. https://doi.org/10.1016/j.jvolgeores.2005.09.005

Srivastava R.P., Vedanti N., Dimri V.P. (2015) New gravity bases in Jabera-Damoh Vindhyan basin, central India. *Journal of the Geological Society of India* 85(3):359-366. https://doi.org/10.1007/s12594-015-0225-4

Tedla G.E., Van Der Meijde M., Nyblade A.A., Van der Meer F.D. (2011) A crustal thickness map of Africa derived from a global gravity field model using Euler deconvolution. *Geophysical Journal International* 187(1):1-9. https://doi.org/10.1111/j.1365-246X.2011.05140.x

Wang G., Zhang S., Yan C., Song Y., Sun Y., Li D., Xu F. (2011) Mineral potential targeting and resource assessment based on 3D geological modeling in Luanchuan region, China. *Computers & Geosciences* 37(12):1976-1988. https://doi.org/10.1016/j.cageo.2011.05.007

Warsi W.E. (1989). Gravity bases in the State of Kuwait. *Journal of the University of Kuwait-Science* 16(2):433-447

Wehr H., Chevrot S., Courrioux G., Guillen A. (2018) A three-dimensional model of the Pyrenees and their foreland basins from geological and gravimetric data. *Tectonophysics* 734:16-32. https://doi.org/10.1016/j.tecto.2018.03.017

Weidmann C., Gimenez M., Klinger F.L., Alvarez O. (2016) Anomalous values of gravity and magnetism in the western margin of Gondwana. *Tectonophysics* 667:1-15. https://doi.org/10.1016/j.tecto.2015.11.017

Xypolias P., Kokkalas S., Skourlis K. (2003) Upward extrusion and subsequent transpression as a possible mechanism for the exhumation of HP/LT rocks in Evia Island (Aegean Sea, Greece). *Journal of Geodynamics* 35(3):303-332. https://doi.org/10.1016/S0264-3707(02)00131-X